Fisheries and Oceans Canada | Pêches et Océans Canada
Ecosystems and Oceans Science | Sciences des écosystèmes et des océans

Canadian Science Advisory Secretariat (CSAS)

Research Document 2021/072

Maritimes Region

Meteorological, Sea Ice, and Physical Oceanographic Conditions in the Labrador Sea during 2019

Igor Yashayaev, Ingrid Peterson, and Zeliang Wang

Fisheries and Oceans Canada
Ocean and Ecosystem Sciences Division
Bedford Institute of Oceanograph
P.O. Box 1006, 1 Challenger Drive
Dartmouth, Nova Scotia B2Y 4A2

December 2021

Canada

Foreword

This series documents the scientific basis for the evaluation of aquatic resources and ecosystems in Canada. As such, it addresses the issues of the day in the time frames required and the documents it contains are not intended as definitive statements on the subjects addressed but rather as progress reports on ongoing investigations.

Published by:

Fisheries and Oceans Canada
Canadian Science Advisory Secretariat
200 Kent Street
Ottawa ON K1A 0E6

http://www.dfo-mpo.gc.ca/csas-sccs/
csas-sccs@dfo-mpo.gc.ca

ISSN 1919-5044
ISBN 978-0-660-40885-9 Cat. No. Fs70-5/2021-072E-PDF

Correct citation for this publication:

Yashayaev, I., Peterson, I., and Wang, Z. 2021. Meteorological, Sea Ice and Physical Oceanographic Conditions in the Labrador Sea during 2019. DFO Can. Sci. Advis. Sec. Res. Doc. 2021/074. iv + 38 p.

Aussi disponible en français :

Yashayaev, I., Peterson I. et Wang Z. 2021. Conditions météorologiques, état de la glace de mer et conditions océanographiques physiques dans la mer du Labrador en 2019. Secr. can. de consult. sci. du MPO. Doc. de rech. 2021/074. iv + 40 p.

TABLE OF CONTENTS

ABSTRACT

In the Labrador Sea, the coldest and freshest North Atlantic basin south of the Greenland-Iceland-Scotland Ridge, wintertime surface heat losses result in the formation of dense waters that play an important role in ventilating the deep ocean and driving the global ocean overturning circulation. In the winter of 2018–2019, the central Labrador Sea gave out less heat through its surface than in any of the five preceding winters. The recent reduction in the seasonal cooling of the Labrador Sea contrasts a 25-year record high winter heat lost in 2015. The winter (December–March) North Atlantic Ocillation (NAO) index was moderately positive in 2019. However, atmospheric circulation associated with a low-atmospheric-pressure anomaly in the Labrador Sea in winter resulted in above-normal air temperatures in the northern and central Labrador Sea. Sea-surface temperatures were near-normal in winter and above-normal in spring. Sea-ice-extent anomalies in winter and spring were generally negative, except for a near-normal winter anomaly on the central Labrador Shelf. With respect to annually-averaged, temperature-anomaly values, in 2018, the upper 100 m layer of the central Labrador Sea was the coldest since 2000. However, between 2018 and 2019, this layer warmed by 0.5 °C. The intermediate (200–2,000 m) layer cooled between 2011 (the layer's warmest year since 1972) and 2018. This cooling trend can be associated with persistent deepening of winter convection over the same time period. The key factor that has contributed to the recurrent deepening of convective mixing in the three winters following the winter of 2015 was not as much air-sea heat exchange as it was the water-column preconditioning caused by convective mixing in the previous years. Such multiyear persistence of deepening winter convection, which lasted until the winter of 2018–2019 and exceeded 2,000 m in depth, has resulted in the most voluminous, densest, and deepest formation of Labrador Sea Water since 1994. In the winter of 2018–2019, the situation has, however, changed with winter convection not generally exceeding 1,200 m and the intermediate layer warming slightly but enough to reverse the seawater-density trend. Between 2018 and 2019, the annual mean-intermediate-layer density reduced by 0.007 kg/m^3. Overall, the changes in the depth of winter convection and intermediate-layer properties between these years imply that the effect of the water-column preconditioning on winter convection has weakened since 2018. Bedford Institute of Oceanography North Atlantic Model simulations suggest that the transport of the Labrador Current decreased between 1995 and 2014, but has since increased slightly. The Atlantic Meridional Overturning Circulation index based on this model demonstrates a general weakening trend since mid-1990s, and continued weakening in recent years is present in this model hindcast.

INTRODUCTION

The Labrador Sea is located between Greenland and the Labrador coast of eastern Canada. Its deep, semi-enclosed basin is bounded by the West Greenland and the Newfoundland-Labrador shelves. Cold, low-salinity waters of polar origin circle the Labrador Sea in a counterclockwise current system that includes both the northward flowing West Greenland Current (WGC) on the eastern side and the southward flowing Labrador Current (LC) on the western side (Figure 1). Much warmer and saltier patches of water can be found under the offshore extensions of the WGC and LC. These are variations of the Atlantic Water originating in the low latitudes of the Atlantic Ocean, and following first the North Atlantic Current and then the Gulf Stream. As the Atlantic Water flows into and around the Labrador Sea, following its eastern, northern, and eventually western boundaries, it mixes with other masses, progressively cooling and freshening.

Spatial distribution and temporal changes in temperature, salinity, density, dissolved oxygen, and other environmental variables in the upper and deep layers of the Labrador Sea respond to a wide range of external and internal oceanic factors. The external factors include exchanges with land (e.g., continental runoff) and atmosphere (e.g., radiation) latent and sensible heat, and momentum fluxes, precipitation, evaporation, and exchanges with other substances (such as anthropogenic gases). The internal factors include inflows of warmer and saltier, and colder and fresher waters from the adjacent North Atlantic and Arctic, respectively, and local oceanic processes such as lateral mixing and winter convection. Naturally, the physical, chemical, and biological processes and seawater properties are subjected, both vertically and horizontally, to seasonal, interannual, and decadal variations across the region. In addition, instantaneous conditions and process development depend on the cumulative effect of past heat, salt, and freshwater gains and respective temperature, salinity, and density changes termed as ocean preconditioning (Yashayaev and Loder 2017).

Since 1990 except for 2017, the Bedford Institute of Oceanography (BIO) has been conducting annual occupations of the oceanographic section Atlantic Repeat 7-West (AR7W). This section spanning the Labrador Sea (Figure 1, Table 1), was first included as both one-time (A1E) and repeat (AR7W) hydrographic lines in the World Ocean Circulation Experiment (WOCE) array (Lazier et al. 2002, Kieke and Yashayaev 2015a, Yashayaev et al. 2015). Later, the observations collected on the AR7W line became and presently remain an important contribution of Canada to the international Global Climate Observing System (GCOS), the Climate Variability (CLIVAR) component of the World Climate Research Programme (WCRP), and the Global Ocean Ship-based Hydrographic Investigations Program (GO-SHIP).

The annual multidisciplinary survey of AR7W, presently conducted as the core component of the Atlantic Zone Off-shelf Monitoring Program (AZOMP) of Fisheries and Oceans Canada (DFO), has been highlighted in numerous high-impact publications (e.g., Dickson et al. 2002, Curry et al. 2003, Thornalley et al. 2018, Lozier et al. 2019, Fröb et al. 2016, Holliday et al. 2020), special journal issues (e.g., Yashayaev 2007b, Yashayaev et al. 2015a, Yashayaev et al. 2015b and Kieke and Yashayaev 2015), books (e.g., Dickson et al. 2008), the Fourth and Fifth Assessment Reports (AR) of the Intergovernmental Panel on Climate Change (IPCC, e.g., Bindoff et al. 2007, Rhein et al. 2013), the International Council for the Exploration of the Sea's (ICES's) Reports on Ocean Climate (IROC) (e.g., González-Pola et al. 2020) and Northwest Atlantic Fisheries Organization (NAFO) reports (e.g., Yashayaev et al. 2020).

The annually-visited Labrador Sea oceanographic section AR7W spans approximately 900 km from Misery Point, Labrador, to Cape Desolation, Greenland. With exactly three decades of coast-to-coast, surface-to-bottom observations methodically collected on AR7W during the

period from June of 1990 through June of 2019, we are able to construct and analyze long-term trends in all key ecosystem variables, except for those affected by the seasonal cycle unresolved in one-per-year snapshots spread over the May–July period. It should also be noted that the seasonal spread of observations was not random throughout the entire period, adding a systematic bias to estimates of long-term changes in seawater properties based on the shipboard measurements in the upper layer. Since 1995, the mid-point date of the AR7W survey has occurred between early May and late July, with the earliest dates occurring since 2014, and the latest dates occurring before 2004 (Table 1). These sampling limitations make interannual and longer-term variability unresolvable in biological variables based on the shipboard samples as discussed in *Synthesis of Multiplatform Data Sets*. However, the variability in survey date may be helpful in determining the seasonal cycles in different regions of the sea (Fragoso et al. 2016). As shown in the *Appendix*, for physical variables, the variability in survey date has a significant effect near the surface (0–100 m), exceeding standard deviation of anomalies, but little effect at depths greater than 200 m. In order to report the interannual and longer-term variability of the physical variables throughout the entire water column, surface-to-bottom, the seasonal cycle has been removed from data for all depths.

In addition to irregular seasonal coverage, there are limitations imposed on interpretations of oceanographic data collected on the shelf and even slope segments of the AR7W line by insufficient spatial coverage due to moderate-to-heavy sea-ice conditions in some years. As a result, the near-coastal stations cannot always be reached, making the shelves and, in a number of cases, the continental slopes more limited in data coverage than the deeper regions, thereby creating spatial shifts in data distribution in high-horizontal-gradient boundary regions.

Additionally, the scope of the DFO-led deep-water monitoring activities includes occupations of the Extended Halifax line, maintaining deep-water oceanographic moorings in the Labrador Sea and on the Scotian Slope and deployments of profiling Argo floats in both regions.

Numerical model simulations are instrumental in connecting the changes in water mass characteristics and boundary current systems.

The following four sections (meteorological, remotely-sensed sea surface temperature, sea ice, water-column temperatures and salinities, and numerical model results) are observation or model specific. Each of these sections starts with brief descriptions of data and methods.

This document is in support of the AZMP Science Advisory Report (DFO 2020).

METEOROLOGICAL OBSERVATIONS

NORTH ATLANTIC OSCILLATION (NAO) INDEX

The NAO is an important teleconnection pattern influencing atmospheric processes in the Labrador Sea (Barnston and Livezey 1987, Hauser et al. 2015). When the North Atlantic Oscillation (NAO) is in its positive phase, low-pressure anomalies over the Icelandic region and throughout the Arctic combined with high-pressure anomalies over the Azores and across the subtropical Atlantic produce stronger-than-average westerlies across the mid-latitudes. Conditions over the northwestern Atlantic, including the Labrador Sea region, are colder and drier than average. A negative NAO indicates a relative weakening of either the Icelandic low or the Azores high, or both, which decreases the pressure gradient across the North Atlantic resulting in weakening of the westerlies and brings warmer conditions than usual. Both NAO phases are associated with basin-wide changes in the intensity and location of the North Atlantic atmospheric jet stream and storm track, and in large-scale modulations of the zonal and meridional heat and moisture transport (Hurrell 1995), resulting in the modification of the

temperature and precipitation patterns. Even though the focus of this report is on the past three decades, we present and analyze the 72-year-long NAO, winter surface heat loss and oceanographic records to relate the recent conditions to the major shifts in the atmospheric situations over the North Atlantic.

NAO indices computed using two versions of the NAO index are shown in Figure 2 (upper panel). The station-based NAO index (green) is the difference in winter (December, January, February, March) sea-level atmospheric pressure between the Azores and Iceland (Hurrell et al. 2018). The Principal Component (PC)-based NAO index (blue) is associated with the first Empirical Orthogonal Function (EOF) of standardized monthly 500-mb height anomaly fields for the Northern Hemisphere. The spatial pattern of this EOF shows a high over southern Greenland, and a low near the latitude of the Azores.

The wintertime NAO exhibits significant multi-decadal variability (Hurrell 1995). An upward trend of the NAO index from the 1960s to the 1990s was noted by Visbeck et al. (2001), although, since the peak in the 1990s, there has been a slight downward trend. Recent studies reveal an atmospheric circulation pattern, complementary to NAO, which becomes more prominent in years of low NAO (Hauser et al. 2015). Further study of this phenomenon will help to improve understanding and forecasting capabilities of atmospheric and oceanic conditions.

In 2010, the NAO index reached a record low (Figure 2, upper panel). In 2011, the NAO index rebounded from the record low but still remained well below the 30-year average (1981–2010). In 2012, however, the NAO index was strongly positive, up to a level comparable to those in early 1990s, showing the highest winter index over the last twenty years. There was a significant change in the winter NAO index in 2013, when it became moderately negative. In 2014, the NAO index returned to its high positive phase, slightly lower than the 2012 value, making it the second highest in the last twenty years. In 2015 there was another high NAO event, the largest positive NAO magnitude in the 122-year-long instrumental record. In 2019, both the station-based NAO anomaly (green) and the PC-based NAO anomaly (blue) were moderately positive, and have decreased from the extremely high values observed in 2015.

Figure 2 also shows maps of the mean Sea Level Pressure (SLP) in winter (December, January, February, March) for the 1981–2010 mean and for 2019 over the North Atlantic (middle panels). In 2019, a westward shift in the Icelandic low toward the Labrador coast can be seen, so that a low-pressure anomaly is present in the Labrador Sea region (bottom left panel). This pattern is associated with a positive northward-vector wind anomaly off southwestern Greenland (bottom right panel).

AIR TEMPERATURES

The air-temperature data used are from the National Centers for Environmental Prediction (NCEP) Reanalysis dataset, provided by the NOAA/OAR/ESRL, PSD (National Oceanic and Atmospheric Administration/Ocean and Atmospheric Research/Earth System Research Laboratory, Physical Sciences Division), Boulder, Colorado, USA. The NCEP Reanalysis is a joint project between the NCEP and the National Center for Atmospheric Research (NCAR). The goal of this joint effort is to produce a new Surface Air Temperature and Sea Surface analysis using historical data (1948 onwards) and to produce analyses of the current atmospheric state (Kalnay et al. 1996).

Time-series plots of winter and spring air-temperature anomalies in the Labrador Basin are shown in Figure 3, for the box 55–60°N, 50.0–52.5°W (Figure 4, left panel). In 2019, air temperatures for both winter and spring were 0.5–1.0 SD above normal. Winter and spring maps of surface-air-temperature anomalies in 2019 from the NCEP Reanalysis are shown in

Figure 4. In the winter map, a positive anomaly can be seen in the northern Labrador Sea, consistent with the low SLP anomaly noted in the previous section.

This low SLP anomaly is associated with a positive northward-vector wind anomaly off southwestern Greenland, which would lead to warmer air flowing northward from the region of warmer oceanic waters to the south. This may be a factor leading to the positive air-temperature anomaly in the northern Labrador Sea. In contrast, a negative air-temperature anomaly is expected to be associated with a positive westerly to northwesterly-vector wind anomaly, bringing colder air from land regions.

In addition, the positive northward-vector wind anomaly off southwestern Greenland may reduce Ekman transport of cold, fresh water from the Greenland shelf into the offshore West Greenland Current (see Luo et al. 2016 and Castelao el al. 2019). This would warm, salten, and weaken the current, which flows northward and then westward into the northern Labrador Sea, and lead to positive Sea Surface Temperature (SST) and salinity anomalies there. Similarly, in the northern Labrador Sea, the easterly wind anomaly may increase (reduce) advection of relatively warm (cold) surface water northward (southward), increasing SST, and reducing sea-ice extent. Increased SST and reduced sea-ice extent may contribute to the positive air-temperature anomaly in the northern Labrador Sea.

AIR-SEA HEAT FLUX

The cumulative air-sea heat flux integrated over individual-year cooling seasons (cumulative winter surface-heat flux/loss in Figures 3 and 9) was computed using 6-hourly heat flux and daily-mean radiation data obtained from the United States (U.S.) National Centers for Environmental Prediction (NCEP) Reanalysis (Kalnay et al. 1996). The two available versions of NCEP Reanalysis products, R1 and R2, are jointly used to provide the most extensive up-to-date data coverage.

The total or cumulative surface heat loss incurred in a cooling season was estimated by integrating the net surface heat flux over the Labrador Basin from start to end of a time period showing continuous cooling. Each fall-to-spring cooling period (also cooling cycle) was defined individually from the first date when the net surface heat flux became consistently positive (sea-to-air) to the moment since when its negative values (air-to-sea) prevailed.

Specifically, the net heat flux values used in this integration were computed as a sum of incoming and outgoing shortwave and longwave radiative, and latent and sensible turbulent heat flux components extracted for the region of interest from the NCEP/NCAR Reanalysis fields. As already noted, the start and end points of each cooling cycle were associated with the net flux reversals in fall and spring (Yashayaev and Loder 2009).

The highest annual heat losses during 1974–2019 were achieved in 1993 and 2015. Since 1998, the top six cumulative surface-heat losses have occurred in 2008, 2012, 2014, 2015, 2016, and 2017. The heat loss in 2019 was the lowest in six consecutive years.

REMOTELY-SENSED SEA SURFACE TEMPERATURE

The Sea Surface Temperature (SST) data used are from the NOAA Optimum Interpolation (OI), SST, version 2 (NOAA_OI_SST_V2) dataset provided by the NOAA/OAR/ESRL PSD, Boulder, Colorado, USA. The Optimum Interpolation Sea Surface Temperature (OISST) analysis is constructed by combining observations from satellites, ships, and buoys on a regular global grid, and interpolating to fill in gaps.

Time-series plots of winter (January–March) and spring (April–June) sea-surface-temperature anomalies in the Labrador Basin (55–60°N, 50.0–52.5°W) are shown in Figure 3. Winter and spring maps of sea-surface-temperature anomalies (Figure 5) show positive anomalies in the northern Labrador Sea, especially in the spring, similar to the air-temperature anomalies. However, unlike air-temperature anomalies, minimum SST anomalies areas are limited by the freezing point of seawater.

SEA-ICE OBSERVATIONS

Sea-ice concentrations derived from satellite passive microwave data since late 1978 are obtained from the U.S. National Snow and Ice Data Center. These data were used instead of Canadian Ice Service (CIS) data because they extend farther east, so that they cover the Greenland shelf (comparisons conducted in support of this report show [not shown] that the anomalies computed from each dataset for the same area agree very closely).

Monthly sea-ice-concentration data are used for 1978–2018 (Cavalieri et al. 1996, Fetterer et al. 2002) and daily real-time data are used for 2019 (Meier et al. 2017). Ice extent is defined as the area in which ice concentration is at least 15%, and is computed for three latitude bands in the Labrador Sea region: 63–68°N (Davis Strait), 58–63°N (Northern Labrador Sea), and 53–58°N (Labrador Shelf). Sea-ice observations for the Labrador Sea region based on CIS ice-chart data are presented in Cyr et al. (2021).

Winter and spring time series of sea-ice-extent anomalies for these three regions are shown in Figure 6, with the locations of the regions shown in Figure 7 (bottom panel). Winter- and spring-ice-extent anomalies in 2019 are negative for all regions, except the winter anomaly for the Labrador shelf, which was near-normal.

Figure 7 shows monthly maps of sea-ice-concentration anomalies (top panel) and extent (middle panel) from January to March 2019, using data from the U.S. National Snow and Ice Data Center. The magenta lines in the lower panel show the median limit of ice extent. In the northern Labrador Sea, negative ice-concentration anomalies can be seen, and the ice extent is lower than normal, in agreement with winter-air-temperature and sea-surface-temperature anomalies.

OCEAN TEMPERATURES AND SALINITIES

SHIPBOARD OBSERVATIONS

Since 2004, the AR7W survey has been carried out mostly in May with at least 30 Conductivity Temperature Depth (CTD)—although a broader range of sensors than these three are used routinely on every deep-sea oceanographic mission—and water sampling (e.g., for dissolved oxygen, nutrients, transient tracers) stations occupied between Labrador and Greenland. The pressure, temperature, conductivity, salinity, and dissolved oxygen data sets have been quality controlled and calibrated to meet WOCE standards, using water sample (e.g., Autosal salinity and Winkler titration), SBE35 temperature recorder and laboratory calibration data. Argo float temperature and salinity profiles, available since 2002, have been quality controlled through comparisons with vessel CTD and water sample data and comparisons between floats, and by performing critical analyses of spatial and temporal deviations. The historical and other recent data have also been quality controlled and processed through similar critical analyses (see Yashayaev and Seidov 2015, for a summary of the data editing and processing approaches used here as well).

The BIO-led Labrador Sea survey data were enhanced with temperature and salinity observations archived by other programs and national and international data centers (e.g., Kieke and Yashayaev 2015).

ARGO PROFILING FLOAT DATA

Argo is an international network of profiling floats collecting high-quality temperature and salinity profiles from the upper 2,000 m of the ice-free global ocean, and through float displacements, currents from intermediate depths. For most of a typical 10-day cycle a battery-powered autonomous float freely drifts at a “parking depth” of usually 1,000 m, where its position is stabilized through buoyancy adjustment. Once the float is released from its parking depth, it descends to approximately 2,000 m and then ascends to the surface, while profiling temperature, salinity, and other variables, if additional sensors are installed. When the surface is reached, the acquired data are transmitted, and the float sinks back to its parking depth. Since 2002, the near real-time temperature and salinity Argo float data collectively draw a large-scale picture of the oceanographic structure and circulation of the Labrador Sea. The array is typically used to reconstruct the seasonal and interannual variability of the physical characteristics and dissolved oxygen in the upper 2,000 m water column. The value of the Argo floats is even more significant in winter, when they serve as the only means of providing information about real-time development of winter convection, and when there are no shipboard measurements available.

Overall, the network of profiling Argo floats provided temperature and salinity data to 2,000 m used for monitoring of year-round variability of the oceanographic conditions in the Labrador Sea. However, the number of the floats within the Labrador Sea during 2019 was just marginally sufficient to resolve sub-monthly variability.

SYNTHESIS OF MULTIPLATFORM DATA SETS

Temperature and salinity data in the Labrador Sea from various sources are compiled and seasonally adjusted to provide individual time series. Our primary data sources include: (1) full-depth-temperature, salinity, and dissolved-oxygen profiles collected on the AR7W line across the Labrador Sea that has been occupied by BIO since 1990, (2) water-sample and discrete-SBE35-temperature data used to calibrate the instrument sensors, (3) temperature and salinity profiles over the upper 2,000 m in the Labrador Sea region from the International Argo float program, (4) publically available observed-level temperature and salinity data from other programs and national and international data centers (e.g., Kieke and Yashayaev 2015), and (5) a near-bottom, moored-temperature time series from a long-term mooring maintained by the BIO on the Labrador continental slope—a respective 30-year series follows the same pattern of interannual temperature changes as the intermediate-depth layer in the central Labrador Sea (Figure 5 in Yashayaev and Loder 2016).

Following Yashayaev and Loder (2009, 2016, and 2017), but now including all available Argo float data up to February 2020 and ship survey data up to June 2019 (Figure 1), time-depth series of spatially-averaged potential temperature, salinity, and potential density with weekly-to-monthly (dependent on Argo and ship survey-data coverage) resolution have been computed for an area of approximately 60,000 km^2 in the central Labrador Sea. To provide for this, all individual CTD, water sample, and Argo float profiles of an analyzed variable selected within the central Labrador Sea contour defined in our earlier studies (e.g., Yashayaev and Loder 2016) were vertically interpolated and aggregated into time series for each depth level included in a chosen layer.

As stated in the *Introduction*, the seasonal cycle dominates the upper-layer variability and extends to the intermediate layer. Therefore, an assessment and, if required, a correction of

seasonal biases are necessary steps in any multiyear data synthesis and analysis. Specifically, at least one of the following conditions must be met to be able to investigate longer-term variability in presence of strong seasonality: (1) the contribution of seasonal cycle to the total variance is less than the contribution of longer-term signals, (2) the seasonal cycle can be effectively removed from analyzed measurements, and (3) the temporal resolution and seasonal coverage of analyzed data is sufficient and consistent through a study period. The *Appendix* includes seasonal cycles of temperature and salinity (Figure A1), associated seasonal changes encountered over 30-day periods (Figure A2), and seasonal changes measured from (relative to) May 15 (Figure A3), standard deviations of multiyear anomalies computed in 10-day bins (Figure A4), and contributions of seasonal cycles to total variances (Figure A5). These figures reveal that the shipboard data collected on the AR7W line over 30 years cannot be used to map interannual variability in both physical and biochemical variables in the top 100 m. The largest seasonal temperature changes are observed in April–June, at the time of the fastest increase in the solar irradiance. The noted seasonal changes exceed the reported interannual variability. To address this issue, the measurements of all physical variables (temperature, salinity, and density) have been corrected, depth by depth, for seasonality by using an iterative procedure obtaining a harmonic representation of the seasonal cycle and removing data outliers. The resulting series have been low-pass-filtered, and the filtered values have been averaged annually to obtain the annual variable values since 1987.

Further, to place the recent variability in a historical context, we use annual time series of temperature, salinity, and density averaged over the 15–100 and 200–2,000 m vertical intervals in the central Labrador Sea back to 1948 as long-term indices of these variables over its upper- and intermediate-depth waters (Figure 9). These were derived from time series for selected depths like those discussed above and previously reported.

WINTER CONVECTION AND HYDROGRAPHIC CONDITIONS IN THE CENTRAL LABRADOR SEA

Long-term Changes in Key Water Masses

Multidecadal time-depth distributions of annual temperature, salinity, and density (referenced to a pressure of 1,000 dbar) values in the central Labrador Sea since 1948 at depths of 200–3,500 m are shown in Figure 8. A combination of averaging on constant-density and constant-pressure surfaces or levels was used in the computational procedure to achieve best representation of annual seawater characteristics. Time-series plots of annual- and spring- (April–June) mean-temperature and salinity values averaged over the 15–100 m and 200– 2,000 m depth ranges are presented in Figure 9.

Hydrographic data transmitted by profiling Argo floats become widespread in 2002, eventually resolving sub-monthly to decadal variability in the top two kilometers of the ocean. Time-depth distributions of temperature, salinity, and density (referenced to a pressure of 1,000 dbar) observations from the sea surface to a depth of 2,000 m averaged over 10-day intervals since 2002 are presented in Figure 10.

The intermediate, deep and abyssal or bottom water masses found in the Labrador Sea are Labrador Sea Water (LSW), Northeast Atlantic Deep Water (NEADW, 2,500–3,000 m), and Denmark Strait Overflow Water (DSOW, defined as a 200 m thick bottommost layer at the water depths exceeding 3,000 m). Similarly to DSOW, NEADW is also derived from the Iceland-Scotland Overflow Water, but undergoes a longer and more substantial mixing, transformation, and modification along its path (Yashayaev and Dickson 2008). While the temporal changes within NEADW are comparably slow, typically spanning a few decades, and

appear to be vertically-uniform (note how NEADW salinity changed 1975 to 2001 to present in Figure 8), both LSW and DSOW exhibit strong variations on decadal and shorter time scales.

Recurring warm and saline, and cold and fresh events spread in the upper 2,000 m layer, mainly occupied by LSW. In over 90 years of direct oceanographic observations (Figure 8 and Figure 9, earlier years are not included), the intermediate, 200–2,000 m, layer of the Labrador Sea experienced three periods of sustained cooling of the entire layer separated by two periods of warming. The first cooling event took place in the 1950s, followed by a warming and salinification trend through the early 1970s, bringing the sea to its record warm and saline state. Then the layer started to cool to reach its all-time cold record in 1994. The warming period that followed showed a steady temperature growth until the second warm peak was reached in 2011. Similarly to the period of warming that ended in the early 1970s, the recent warm state did not last very long either. Similarly to the earlier two periods (in the 1950s and 1990s) of sustained cooling of the intermediate layer, the cooling that followed the second warming period came as a direct result of persistently deepening convection during the winters from 2012 through 2018. Indeed, the lowest sea-average temperature and salinity values were those achieved with cooling and freshening of LSW culminating in the late 1980s to mid-1990s. This period was characterized by deep winter convection that filled the upper 2,000–2,500 m layer of the Labrador Sea with cold, dense, and relatively fresh water. Milder winters in the early 2000s produced more limited amounts of LSW, which have gradually become warmer, saltier, and less dense than in the previous decade (Yashayaev 2007a). The positive-temperature and negative-density trends established in the top 1,000 m of the sea following the cessation of extreme convection in the mid-1990s were repeatedly interrupted by moderately deep convection in the winters of 1999–2000, 2002 (Figure 8), 2008, and 2012 (Figure 8 and Figure 10). Most of these warming-trend reversals were short-lived, except for the latest (in 2014), discussed in more detail in the next section.

Both upper, 15–100 m, and deeper, 200–2,000 m, layers were mainly cooling since 2010, reaching their lowest temperatures in 2018 and warming afterward, namely, through 2019. However, the tendency turning point in salinity did not match that in temperature—the freshening trend seen in the newly-formed or newly-ventilated LSW between 2011 and 2016, reversed in 2016, making the LSW formed in the winter of 2018 the densest since the mid-1990s.

The cooling trends of the upper and intermediate layers reversed in 2019 as the amount of heat transferred from the ocean to the atmosphere in the winter of 2019 was the lowest since 2013. The recent warming of the upper and intermediate layers of the Labrador Sea concurs with the reduced heat loss and shallowed convection in the winter of 2019.

To interpret the changeovers in cooling and warming states of the Labrador Sea, Figure 9 also includes the winter NAO and cumulative winter surface heat flux (because the ocean loses heat through each cooling season, this metric can also be regarded as cumulative heat loss). Their low-pass filtered values (centered on the last year of the filter window) represent the combined effect of recent surface heat losses and water column preconditioning in previous years.

Recent Seasonal and Interannual Variability in the Upper 2,000 m

The particularly long positive-temperature and negative-density trends in the intermediate layer (200–2,000 m) that lasted for about two decades starting in the mid-1990s (Figures 8–10) kept resuming their previous rates soon after each interruption. However, the multiyear persistence of these trends came to the end in the winter of 2014, when deep convection reaching 1,500 m and deeper spanned a considerable part of the Labrador Basin reversing the signs of

year-to-year changes in both temperature (to negative) and density (to positive) leading to sustained cooling and density increase over this and the following four years.

Deep convection has deepened progressively over the five consecutive winters—2014 through 2018. During this period, each convective development produced a colder denser and deeper LSW than the preceding event. As a result, the convectively formed water mass, LSW, was getting colder and denser as convection deepened between 2014 and 2018, inclusively. Overall, the progressive cooling of the top 2,000 m, and deep and intense winter mixing during the five consecutive winters of 2014 through 2018 have interrupted the general warming and stratification-building trend that has persisted in the intermediate waters of the Labrador Sea since the mid-1990s.

The deep convection event of 2008 is evident in both the temperature and salinity fields. The depth of shallower convection in 2009 was partly reduced because of massive surface freshening in the preceding summer and fall. The conditions in the winter of 2011 were similar to those in the preceding winter with very limited convection (mixed layer depths did not exceed 800 m). Then, in the winter of 2012, convection reached the depths of approximately 1,400 m, which is clearly present in temperature and salinity profiles acquired by both Argo floats and ship survey. Salinity in the top 200 m in 2012 was the lowest since 2003, particularly in the top 50 m. Convection also occurred in the winter of 2013, but it was not as deep as in the previous year, and was mostly limited to the top 1,000 m. The situation changed quite significantly in the winter of 2014. Wintertime cooling triggered convective mixing, homogenizing the top 1,600 m (and probably even deeper) layer in the central Labrador Sea. As mentioned earlier, winter convection progressed over the following four years reaching deeper and making the top 2,000 m layer colder and denser with every cooling cycle. In the last of these winters, convection reached and exceeded the depth of 2,000 m. These persistent trends in temperature (negative), density (positive) and convection depth (positive), spanning 2011–2018 (Figures 8–10), were caused by a multiyear recurrence of relatively strong, but not necessarily extreme, winter cooling, typically coinciding with moderate-to-high positive NAO. The multiyear cooling led to convective preconditioning of the water column in such a way that winter convection continued to deepen even in reduced winter cooling situation. The winter of 2018 has set a good and presently last example of how a preconditioning of a deep basin reservoir in preceding years may affect convection in a current year, further supporting the hypothesis by Yashayaev and Loder (2017). As in the previous two winters, in the winter of 2018, the subpolar North Atlantic basins lost considerably lesser amounts of heat to surface cooling than in the winter of 2015 (the latter demonstrated the highest cumulative surface heat loss in more than two decades). With the exception of the last winter on record (2019), the cumulative 2018 winter heat loss was also the lowest in the Labrador Sea since the winter of 2014. However, despite the continual reduction in winter cooling, the steady increase in the depth of winter convection since 2015 has resulted in the development of the most significant, in terms of volume, depth, and density, class of LSW since 1994.

The cumulative 2019 winter heat loss was only slightly less in magnitude than in the previous winter. Yet, unlike the five preceding cases, the last winter brought a rather weak convection, setting a limit to the preconditioning endorsement/enhancement of current-year winter convection discussed in our report earlier.

The persistence in deep convective mixing contributing to the massive LSW development in the recent years and the recent cessation of deep convection are effectively shown in the temporal progression of cascading vertical temperature, salinity and density profiles (Figure 10) as the cold, dense water reaches deeper and deeper with time, and then, in 2019 the trend reverses. Each of the freshly-made deepened and densified LSW vintages was in part preserved in the deep basin until the next winter. This figure illustrates the essence of water column

preconditioning by winter convection—sustaining or “memorizing” the previous year conditions throughout the intermediate depths at the convection site same as in the previous report. Yet the added year enriches the progression showing a reversal in positive development in winter mixing.

In addition to surface heat flux, another factor that could potentially change convection is surface freshening due to accelerated melting of the Greenland Ice Sheet. However, a recent study by Dukhovskoy et al. (2019) indicates that the effect of the Greenland freshwater-flux anomaly brought by the observed acceleration of Greenland Ice Sheet melt is not sufficient to fully explain the present changes in water column salinity and convective activity. In fact, there is no significant negative trend present in surface salinity in the Labrador Basin in the last decade.

Turning Points in the Progressive Development of Winter Convection and Trends of Oceanographic Characteristics Defined with High-Frequency Observations

This section focuses on the recent change in convective activity in the Labrador Sea, its cause and appearances in physical and chemical seawater properties.

The sub-monthly temperature, salinity, and density data (Figure 10, 2002–2020 with effective temporal resolution of 5–10 days) show that the winter mixed layer and hence convection in the central Labrador Sea reached and even exceeded 2,000 m in March of 2018, ending the sustained positive trend in convection depth spanning the winters of 2012 and 2018 except for 2013. The last three winters in this sequence have demonstrated that certain extreme properties, such as low temperature, weak vertical stability, and weak overall stratification, imposed on the water column by a stronger-than-usual convective mixing in the previous years, may assist further development of deep convection. In order to reveal and diagnose long-term, water-column preconditioning situations such as the one presented here, continuous year-round measurements of temperature and salinity are required. For example, the recent successive deepening of winter mixing (Figure 10) appears as a significant feature in longer-term reconstructions (Figures 8 and 9), yet its true origin and vertical and temporal developments can only be unambiguously mapped with higher-resolution data.

Despite comparable surface heat losses, convection in the winter of 2019 was much shallower than in the winter of 2018. This negative change in the convection depth (positively) adds to our understanding of the recurrent nature of deep convection. It shows when the past-winter preconditioning of the water column loses its significance for development of convection in present and future winters. Indeed, while convection continued to exceed 1,500 m and even deepen over the three years first after the surface heat losses started to decline (since the winter of 2015), it happened only on the fourth year when the intensity and depth of winter convection picked the trend in the surface heat loss. It was not the first time when a deep-water preconditioning had a prolonged effect on convection in the Labrador Sea. A similar situation was observed in the 1987–1996 time period. Despite a decline in atmospheric forcing from the previous winter, the Labrador Sea experienced deep convection (> 2,000 m) in the winter of 1995, whereas there was no deep convection observed in the same basin in the following winter (1996).

Distance-depth plots of temperature, salinity, density, and oxygen from the survey data in 1994, 2011, 2012, 2015, 2018, and 2019 are presented in Figures 11–14. An extensive reservoir filled with a newly ventilated, 2,000 m deep, cold, dense, fresh, atmospheric gas loaded vintage of LSW is clearly evident in the AR7W seawater property section based on the 2018 May shipboard CTD data. The 2018 vintage of LSW is associated with low temperature (< 3.3 °C) and low salinity (< 34.86) between 1,000 and 2,000 m. The winter convection in the recent time

period, 2015–2018, especially in the winter of 2018, is arguably the deepest since the record-deep cooling that reached 2400 m in the winter of 1994. The LSW year class is one of the largest ever observed outside of the early 1990s.

The sections plots (Figures 11–14) further confirm that winter convection has lost its strength in the winter of 2019, reaching the depth of about 1,400 m in the western part of the Labrador Basin, and only about 1,000 m in the central and eastern parts, still affecting the distributions of freshwater (salinity) and gases (dissolved oxygen) across the Labrador Sea, but not in the deep intermediate layer as in the previous years.

NUMERICAL MODEL RESULTS

In this report, an ocean model hindcast from the Bedford Institute of Oceanography North Atlantic Model (BNAM, Brickman et al. 2016, Wang et al. 2016, Brickman et al. 2018, Wang et al. 2018) is used to report changes of the Labrador Current and the Atlantic Meridional Overturning Circulation (AMOC).

The BNAM is based on the NEMO 2.3 (Nucleus for European Modelling of the Ocean) model. It includes an ocean component, OPA (Océan Parallélisé) and a sea ice module LIM (Louvain-la-neuve sea Ice Model). Its domain was selected to include the North Atlantic Ocean (7ºN–75ºN and 100ºW–25ºE) with a nominal resolution of 1/12º. The model has a maximum of 50 levels in the vertical, with level thickness increasing from 1 m at the surface to 200 m at a depth of 1250 m and reaching the maximum value of 460 m at the bottom of the deep basins. The maximum depth represented in the model is 5,730 m.

Open boundary data are from the GLORYS reanalysis product (Global Ocean ReanalYses and Simulations). The model surface forcing is taken from a combination of CORE (Coordinated Ocean-ice Reference Experiments) and NCEP/NCAR reanalysis forcing. Model-forcing variables include air temperature, wind velocities, and humidity; daily short- and long-wave radiation, and total precipitation (rain plus snow). No surface restoring to sea-surface temperature is applied. However, the model's sea-surface salinity is restored to its monthly climatology with a 60-day restoring time scale.

The model was spun-up for 10 years using the CORE normal-year forcing. The 10-year spin-up simulation is initialized with a January climatology of Temperature and Salinity (T-S). The T-S climatology combines the Polar Science Center Hydrographic Climatology (PHC2.1) at high latitudes with the T-S climatology of WOA5 at middle and low latitudes.

The hindcast period is from 1990 to 2019. The barotropic transport is used to represent the strength of the Labrador current. Wang et al. (2016) discovered that the Labrador Current on the shelf break can be partitioned into two portions, and we report the changes of the two branches as well. For the purposes of the present report, the transports were calculated based on modelled flows through the western segment of the AR7W transect.

The AMOC is a climatically important circulation, and it can impact climate at both local and global scales. The BNAM has a decent skill in representing the AMOC (Wang et al. 2019), which allows us to use BNAM to present the variations of the AMOC in this report.

VARIATIONS OF THE LABRADOR CURRENT

The variations of the Labrador Current (LC) can be seen as an indicator for the changes in the subpolar North Atlantic circulation. The variations of the LC are often connected to the variations of the AMOC. Here we present the variations of barotropic transports of the LC.

An EOF analysis of the model output by Wang et al. (2016) presented in Figure 15 suggests that the variability in the Labrador Current can be partitioned into a Western Labrador Current (WLC; from the 300–2,500 m isobaths), and an Eastern Labrador Current (ELC; from the 2,500–3,300 m isobaths). Following the definition of the WLC and ELC, we calculated the transports of ELC and WLC, and also those of the LC (the summation of the ECL and WLC).

The averaged transport over the 1990–2019 period is 45.3 Sv for LC, 19.6 Sv for WLC, 25.7 Sv for ELC. Figure 16 shows the transport anomalies for the LC, ELC and WLC. The WLC in 2019 was marginally weaker than in 2017, about 2 Sv above the 1990–2019 mean, as it has been since 2002

A declining trend of the ELC began in 1996, coinciding with a significant drop in the winter NAO index in the same year. The trend reversed in 2014, and the ELC was approximately 4 Sv stronger in 2019 than in 2018, and it became 1 Sv above the 1990–2019 average.

VARIATIONS OF THE ATLANTIC MERIDIONAL OVERTURNING CIRCULATION

The Atlantic Meridional Overturning Circulation (AMOC) can be presented in two ways—one is in depth space, the other is in density space (Wang et al. 2019). The AMOC reported here is calculated in the depth space. Wang et al. (2019) investigated the variability of the AMOC from the BNAM solution by using EOF approach. Their study proposed the AMOC PC1 as the AMOC index. The AMOC PC1 was found to be representative of the general low-frequency changes of the AMOC, and a general weakening trend was found in the 1990–2015 period. The AMOC PC2 represented the wind-driven Ekman transport portion of the AMOC, which has high-frequency variability and has no obvious trend.

Figure 17 shows a time-latitude plot of the variations of the AMOC from 10°N to 60°N using the monthly mean output from 1990 to 2019, and the seasonal cycle was removed in this calculation A general weakening tendency can be seen in Figure 17. Following the approach in Wang et al. (2019), we applied the EOF approach to the annual mean (de-seasoned) AMOC to compute the EOF patterns and their associated PCs. The EOF1 represents 75% of the total variance, and the EOF2 represents 11%. The EOF patterns are consistent with those in Wang et al. (2019). The AMOC PC1 clearly shows the continuing weakening trend after 2015. No clear trend is shown in the Ekman portion of the AMOC shown in the AMOC PC2. The Labrador Current has been strengthening in recent years as shown above, and the AMOC solution from BNAM still presents the existing weakening trend. The weakening trend of the AMOC in recent years is consistent with Smeed et al. (2018), who used observational data of the AMOC from the RAPID line at 26°N and other observations in their study. The AMOC PC1 shows that the 2019 AMOC is the weakest in the 1990–2019 period.

SUMMARY

The DFO-led annual oceanographic survey of the Labrador Sea provides observations of variability in the ocean climate and ventilation. The changes observed in the region are closely linked to the dynamics of the planetary climate system as a whole and affect the regional climate and ecosystems off Atlantic Canada. In June of 2019, the AR7W line was occupied by the Bedford Institute of Oceanography for the 32nd time since 1990. Additionally, the network of profiling Argo floats provided temperature and salinity data to 2,000 m used for monitoring of year-round variability of the oceanographic conditions in the Labrador Sea. An omission of a single year (as in 2017) in precise systematic observations of the ocean state imposes significant limitation on the assessment, diagnosis and prediction of coast-to-coast, full-depth environmental conditions in one of the most critical locations of the world ocean.

BNAM model results were used to present changes in the Labrador Current (shelf break segment) and the AMOC.

Key characteristics of the past and recent environmental conditions in the Labrador Sea are summarized in the scorecard shown in Figure 19, and are listed below:

1. The winter (December–March) NAO index in 2019 was above-normal. However, a low atmospheric-pressure anomaly in the Labrador Sea in winter resulted in above-normal air temperatures. For SST, anomalies were near-normal in winter and above-normal in spring.
2. Sea-ice-extent anomalies in winter and spring were generally negative, except for a near-normal winter anomaly on the central Labrador Shelf.
3. In the Labrador Sea, surface-heat losses in winter result in the formation of dense waters, which consequently spread across the ocean ventilating its deep layers and essentially driving the global ocean overturning circulation. In the winter of 2015, the Labrador Sea incurred the highest heat loss in more than two decades. However, the four following winters showed a significant reduction in the respective net surface heat losses, which remained above-normal in 2016 and 2017, but then declined to near-normal in 2018 and 2019.
4. Ocean temperature in the central Labrador Sea was above-normal, reversing a negative trend observed since 2010 in the 15–100 m layer, and since 2011 in the 200–2,000 m layer. The earlier cooling of the deeper layer was primarily caused by deepening of winter convection, while the recent warming and convection weakening concur with the reduced 2019 winter heat loss.
5. Despite the persistent decline in the surface cooling since 2015, the water column preconditioned by a series of deep convection events eased the formation of a new LSW that is seen as the most significant, in terms of volume and depth, since the mid-1990s.
6. The temperature and salinity profiles collected by research vessels and profiling Argo floats in the central Labrador Sea indicate that the developed 2019 winter mixed layer was shallower than in the period from 2014 to 2018, during which winter convection incrementally deepened from 1,600 to 2,000 m, respectively, turning out to be the deepest one since 1994 when the 80-year record convection depth of 2,500 m was reached. As a result, the LSW year class developed during the pentad preceding 2019 is among the largest observed outside of the first pentad of the 1990s. In 2019, on the contrary, convection reached the depth of about 1,400 m in the western part of the Labrador Basin, and only about 1,000 m in the central and eastern parts. This also suggests that the near-normal winter convection in the winter of 2019 further added to gas (dissolved oxygen, anthropogenic gases, and carbon dioxide) uptake and consequently respective gas concentrations in the Labrador Sea in the upper 1,000 m layer.
7. Model results suggest that the transport of the Labrador Current decreased between 1995 and 2014, but has since increased slightly. A weakening trend of the AMOC since mid-1990s is obtained in this model hindcast. Continuing weakening of the AMOC in recent years is present, which leads to the weakest AMOC in 2019 from this model simulation.

ACKNOWLEDGEMENTS

We thank the officers and the crews of the Canadian Coast Guard vessels for their dedicated help in keeping the Labrador Sea survey running. We are grateful to the reviewers, Peter Galbraith and Frederic Cyr, for their helpful comments and suggestions. The NCEP Reanalysis data were provided by the NOAA-CIRES Climate Diagnostics Center, Boulder, Colorado, USA, and the sea ice concentration data were provided by the US National Snow and Ice Data Center.

REFERENCES CITED

Barnston, A. G., and Livezey, R. E. 1987. Classification, seasonality and persistence of low-frequency atmospheric circulation patterns. Mon. Wea. Rev. 115: 1083–1126.

Bindoff, N. L., Willebrand, J., Artale, V., Cazenave, A., Gregory, J., Gulev, S., Hanawa, K., Le Quéré, C., Levitus, S., Nojiri, Y., Shum, C. K., Talley, L. D. and Unnikrishnan A. 2007. Chapter 5. Observations: Oceanic Climate Change and Sea Level, Climate Change 2007: The Physical Science Basis, Contribution of Working Group I to the Fourth Assessment Report of the Intergovernmental Panel on Climate Change, [Solomon, S., D. Qin, M. Manning, Z. Chen, M. Marquis, K.B. Averyt, M. Tignor and H.L. Miller (eds.)], Cambridge University Press, Cambridge, United Kingdom and New York, NY, USA.

Brickman, D., Wang, Z., and DeTracy, B. 2016. Variability of Current Streams in Atlantic Canadian Waters: A Model Study. Atmosphere-Ocean, 54 (3): 218–229.

Brickman, D., Hebert, D., and Wang, Z. 2018. Mechanism for the recent ocean warming events on the Scotian Shelf of eastern Canada. Cont. Shelf Res. 156: 11–22.

Castelao, R. M., Luo, H., Oliver, H., Rennermalm, A. K., Tedesco, M., Bracco, A., Yager, P. L., Mote, T. L., & Medeiros, P. M. (2019). Controls on the transport of meltwater from the southern Greenland ice sheet in the Labrador Sea. *Journal of Geophysical Research: Oceans*. 124: 3551–3560.

Cavalieri, D. J., Parkinson, C.L., Gloersen, P., and Zwally, H.J. 1996. updated yearly. *Sea Ice Concentrations from Nimbus-7 SMMR and DMSP SSM/I-SSMIS Passive Microwave Data, Version 1*. [north/monthly]. Boulder, Colorado USA. NASA National Snow and Ice Data Center Distributed Active Archive Center.

Curry, R., R.R. Dickson, and I. Yashayaev, 2003. A change in the freshwater balance of the Atlantic Ocean over the past four decades. Nature. 426: 826–829.

Cyr, F., Colbourne, E., Galbraith, P.S., Gibb, O., Snook, S., Bishop, C., Chen, N., Han, G., and D. Senciall. 2021. Physical Oceanographic Conditions on the Newfoundland and Labrador Shelf during 2019. DFO Can. Sci. Advis. Sec. Res. Doc. 2021/017 iv + 52 p.

DFO, 2020. Oceanographic conditions in the Atlantic zone in 2019. DFO Can. Sci. Advis . Sec. Sci. Advis. Rep. 2020/028.

Dickson, R.R., I. Yashayaev, J. Meincke, W.R. Turrell, S.R. Dye, and J. Holfort, 2002. Rapid freshening of the deep North Atlantic Ocean over the past four decades. Nature. 416: 832–837.

Dickson R.R, Meincke, J., Rhines, P., (Eds.). 2008. Arctic-Subarctic Ocean Fluxes: Defining the Role of the Northern Seas in Climate, Springer Science & Business Media, March 4, 2008, 736 pages.

Dukhovskoy D. S., I. Yashayaev, A. Proshutinsky, J. L. Bamber, I. L. Bashmachnikov, E. P. Chassignet, C. M. Lee and A. J. Tedstone. 2019. Role of Greenland Freshwater Anomaly in the Recent Freshening of the Subpolar North Atlantic. Journal of Geophysical Research: Oceans. 124 (5): 3333–3360.

Fetterer, F., Knowles, K., Meier, W. and Savoie, M. 2002. Updated 2011. Sea ice index. Boulder, CO: National Snow and Ice Data Center. Digital media.

Fragoso, G.M., Poulton, A.J., Yashayaev, I., Head, E.J.H., Stinchcombe, M., and Purdie, D.A. 2016. Biogeographical patterns and environmental controls of phytoplankton communities from contrasting hydrographical zones of the Labrador Sea, Progress in Oceanography. 141: 212–226.

Fröb, F., Olsen, A., Våge, K., Moore, K., Yashayaev, I., Jeansson, E., and Rajasakaren, B. 2016. Irminger Sea deep convection injects oxygen and anthropogenic carbon to the ocean interior. Nat. Commun. 7, 13244

González-Pola, C., Larsen, K. M. H., Fratantoni, P., and Beszczynska-Möller, A. (Eds.). 2020. ICES Report on Ocean Climate 2019. ICES Cooperative Research Reports. No. 350. 136 p.

Hauser, T., Demirov, E., Zhu, J., and Yashayaev, I. 2015. North Atlantic atmospheric and ocean inter-annual variability over the past fifty years—Dominant patterns and decadal shifts. Progress in Oceanography. 132: 197–219.

Holliday, N.P., Bersch, M., Berx, B., Chafik, L., Cunningham, S., Florindo-López, C., Hátún, H., Johns, W., Josey, S.A., Larsen, K.M.H., Mulet, S., Oltmanns, M., Reverdin, G., Rossby, T., Thierry, V., Valdimarsson, H., and Yashayaev, I. 2020. Ocean circulation causes the largest freshening event for 120 years in eastern subpolar North Atlantic. Nat. Commun. 11: 585.

Hurrell, J.W. 1995. Decadal trends in the North Atlantic Oscillation: Regional temperatures and precipitation. Science. 269: 676–679.

Hurrell, J. W. and National Center for Atmospheric Research Staff (Eds). (Last modified 04 Aug 2018). The Climate Data Guide: Hurrell North Atlantic Oscillation (NAO) Index (station-based).

Kalnay, E., Kanamitsu, M., Kistler, R., Collins, W., Deaven, D., Gandin, L., Iredell, M., Saha, S., White, G., Woollen, J., Zhu, Y., Chelliah, M., Ebisuzaki, W., Higgins, W., Janowiak, J., Mo, K.C., Ropelewski, C., Wang, J., Leetmaa, A., Reynolds, R., Jenne, R., and Joseph, D. 1996. The NCEP/NCAR 40-Year Reanalysis Project. Bull. Amer. Meteor. Soc. 77 (3): 437–470.

Kieke, D., and Yashayaev, I. 2015. Studies of Labrador Sea Water formation and variability in the subpolar North Atlantic in the light of international partnership and collaboration. Progress in Oceanography. 132: 220–232

Lazier, J. R. N., Hendry, R. M., Clarke, R. A., Yashayaev, I., and Rhines, P. 2002. Convection and restratification in the Labrador Sea,1990–2000. Deep Sea Res., Part 1. 49: 1819–1835.

Lozier, M.S., Li, F., Bacon, S., Bahr, F., Bower, A.S., Cunningham, S.A., de Jong, M.F., de Steur, L., deYoung, B., Fischer, J., Gary, S. F., Greenan, B. J. W., Holliday, N. P., Houk, A., Houpert, L., Inall, M. E., Johns, W. E., Johnson, H. L., Johnson, C., Karstensen, J., Koman, G., Le Bras, I. A., Lin, X., Mackay, N., Marshall, D. P., Mercier, H., Oltmanns, M., Pickart, R. S., Ramsey, A. L., Rayner, D., Straneo, F., Thierry, V., Torres, D. J., Williams, R. G. , Wilson, C., Yang, J., Yashayaev, I., and Zhao, J. 2019. A sea change in our view of overturning in the subpolar North Atlantic. Science. 363 (6426): 516–521.

Luo, H., Castelao, R., Rennermalm, A., Tedesco, M., Bracco, A., Yager, P. L., Mote, T. L. 2016. Oceanic transport of surface meltwater from the southern Greenland ice sheet. Nature Geosci. **9:** 528–532.

Meier, W. N., Fetterer, F., and Windnagel, A. K. 2017. Near-Real-Time NOAA/NSIDC Climate Data Record of Passive Microwave Sea Ice Concentration, Version 1. [north/daily].

Rhein, M., S.R. Rintoul, S. Aoki, E. Campos, D. Chambers, R.A. Feely, S. Gulev, G.C. Johnson, S.A. Josey, A. Kostianoy, C. Mauritzen, D. Roemmich, L.D. Talley and F. Wang. 2013. Observations: Ocean. In: Climate Change 2013: The Physical Science Basis. Contribution of Working Group I to the Fifth Assessment Report of the Intergovernmental Panel on Climate Change [Stocker, T.F., D. Qin, G.-K. Plattner, M. Tignor, S.K. Allen, J. Boschung, A. Nauels, Y. Xia, V. Bex and P.M. Midgley (eds.)]. Cambridge University Press, Cambridge, United Kingdom and New York, NY, USA.

Smeed, D. A., Josey, S. A., Beaulieu, C., Johns, W. E., Moat, B. I., Frajka-Williams, E., Rayner, D., Meinen, C. S., Baringer, M.O., Bryden, H.L., and McCarthy, G.D. 2018. The North Atlantic Ocean is in a State of Reduced Overturning. Geophysical Research Letters. 45: 1527–1533.

Thornalley, D.J.R., Oppo, D.W., Ortega, P., Robson, J.I., Brierley, C.M., Davis, R., Hall, I.R., Moffa-Sanchez, P., Rose, N.L., Spooner, P.T., Yashayaev, I., Keigwin., L.D. 2018. Anomalously weak Labrador Sea convection and Atlantic overturning during the past 150 years. Nature. 556 (7700): 227.

Visbeck, M.H., Hurrell, J.W., Polvani, L., and Cullen, H.M. 2001. The North Atlantic Oscillation: Past, Present and Future. Proc. Nat. Acad. Sci. 98: 12876–12877.

Wang, Z., Brickman, D., Greenan, B., and Yashayaev, I. 2016. An abrupt shift in the Labrador Current System in relation to winter NAO events. Journal of Geophysical Research Oceans. 121: 5338–5349.

Wang, Z., Lu, Y., Greenan, B., Brickman, D., and DeTracey, B. 2018. BNAM: An eddy-resolving North Atlantic Ocean model to support ocean monitoring. Can. Tech. Rep. Hydrogr. Ocean. Sci. 327: vii + 18p.

Wang, Z., D. Brickman, and B. Greenan, 2019. Characteristic evolution of the Atlantic Meridional Overturning Circulation from 1990 to 2015: An eddy-resolving ocean model study. Deep Sea Research Part I, Oceanographic Research Papers. 149.

Yashayaev, I. M., and I. I. Zveryaev, 2001: Climate of the seasonal cycle in the North Pacific and the North Atlantic Oceans. *Int. J. Climatol.*, **21**, 401–417.

Yashayaev, I. 2007a. Hydrographic changes in the Labrador Sea, 1960–2005, Progress in Oceanography, 73, 242–276.

Yashayeav, I. (Ed). 2007b. Observing and Modelling Ocean Heat and Freshwater Budgets and Transports. Progress in Oceanography. 73 (3–4): 203–426.

Yashayaev, I., and Dickson, R. R. 2008. Chapter 21. Transformation and Fate of Overflows in the northern North Atlantic, Arctic-Subarctic Ocean Fluxes: Defining the Role of the Northern Seas in Climate. R.R.Dickson, J.Meincke, P.Rhines (Eds.), Springer Science + Business Media B.V. 505–506.

Yashayaev, I., and Loder, J.W. 2009. Enhanced production of Labrador Sea Water in 2008. Geophys. Res. Lett., 36 (1).

Yashayaev, I., and Seidov, D. 2015. The role of the Atlantic Water in multidecadal ocean variability in the Nordic and Barents Seas. Progress in Oceanography. 132: 68–127.

Yashayaev, I., Seidov, D., and Demirov, E. 2015a. A new collective view of oceanography of the Arctic and North Atlantic basins. Progress in Oceanography. 132:1–21.

Yashayaev, I., Seidov, D., and Demirov, E. (Eds.). 2015b. Oceanography of the Arctic and North Atlantic Basins. Progress in Oceanography. 132: 1–352.

Yashayaev, I., and Loder, J.W. 2016. Recurrent replenishment of Labrador Sea Water and associated decadal-scale variability. Journal of Geophys. Res. Oceans. 121 (11): 8095–8114.

Yashayaev, I., and Loder, J.W. 2017. Further intensification of deep convection in the Labrador Sea in 2016. Geophysical Research Letters. 44 (3): 1429–1438.

Yashayaev, I., Peterson, I., and Wang, Z. 2020. Meteorological, Sea Ice, and Physical Oceanographic Conditions in the Labrador Sea during 2019. NAFO SCR Doc.20/037, N7085.

TABLES

Table 1. Oceanographic Labrador Sea cruises conducted by the Bedford Institute of Oceanography since 1990 in support of the WOCE, CLIVAR and other international and departmental ocean climate monitoring and research programs

Cruise Name	Vessel	Project	Chief Scientist	Cruise Dates
HUD-92-014	CCGS Hudson	WOCE	John Lazier	27-May–15-Jun, 1992
HUD-95-011	CCGS Hudson	WOCE	John Lazier	7-Jun–5-Jul, 1995
HUD-96-006	CCGS Hudson	WOCE	John Lazier	10-May–2-Jun, 1996
HUD-96-026	CCGS Hudson	WOCE	Allyn Clarke	15-Oct–20-Nov, 1996
HUD-97-009	CCGS Hudson	WOCE/JGOFS	Allyn Clarke	9-May–12-Jun, 1997
HUD-98-023	CCGS Hudson	WOCE/CLIVAR	John Lazier	22-Jun–10-Jul, 1998
HUD-99-022	CCGS Hudson	Climate	Allyn Clarke	27-Jun–14-Jul, 1999
HUD2000009	CCGS Hudson	Climate	Allyn Clarke	20-May–8-Jun, 2000
HUD2001022	CCGS Hudson	Climate	Allyn Clarke	30-May–15-Jun, 2001
HUD2002032	CCGS Hudson	Climate	Allyn Clarke	23-Jun–19-Jul, 2002
HUD2002075	CCGS Hudson	Biology/Climate	Erica Head	29-Nov–12-Dec, 2002
HUD2003038	CCGS Hudson	Climate	Allyn Clarke	13-Jul–4-Aug, 2003
HUD2004016	CCGS Hudson	Climate	Allyn Clarke	14-May–30-May, 2004
HUD2005016	CCGS Hudson	Climate	Allyn Clarke	27-May–7-Jun, 2005
HUD2006019	CCGS Hudson	Climate	Ross Hendry	24-May–8-Jun, 2006
HUD2007011	CCGS Hudson	Climate	Ross Hendry	10-May–29-May, 2007
HUD2008009	CCGS Hudson	Climate	Glen Harrison	20-May–4-Jun, 2008
HUD2009015	CCGS Hudson	AZOMP	Glen Harrison	18-May–1-Jun, 2009
HUD2010014	CCGS Hudson	AZOMP	Glen Harrison	13-May–30-May, 2010
HUD2011009	CCGS Hudson	AZOMP	Igor Yashayaev	6-May–29-May, 2011
MLB2012001	CCGS M.L. Black	AZOMP	Igor Yashayaev	25-Jun–20-Jul, 2012
HUD2013008	CCGS Hudson	AZOMP	Igor Yashayaev	4-May–28-May, 2013
HUD2014007	CCGS Hudson	AZOMP	Igor Yashayaev	2-May–26-May, 2014
HUD2015006	CCGS Hudson	AZOMP	Igor Yashayaev	1-May–26-May, 2015
HUD2016006	CCGS Hudson	AZOMP	Igor Yashayaev	30-Apr–24-May, 2016
HUD2018008	CCGS Hudson	AZOMP	Igor Yashayaev	25-Apr–20-May, 2018
AMU2019001	CCGS Amundsen	AZOMP	Igor Yashayaev	2-Jun–19-June, 2019

FIGURES

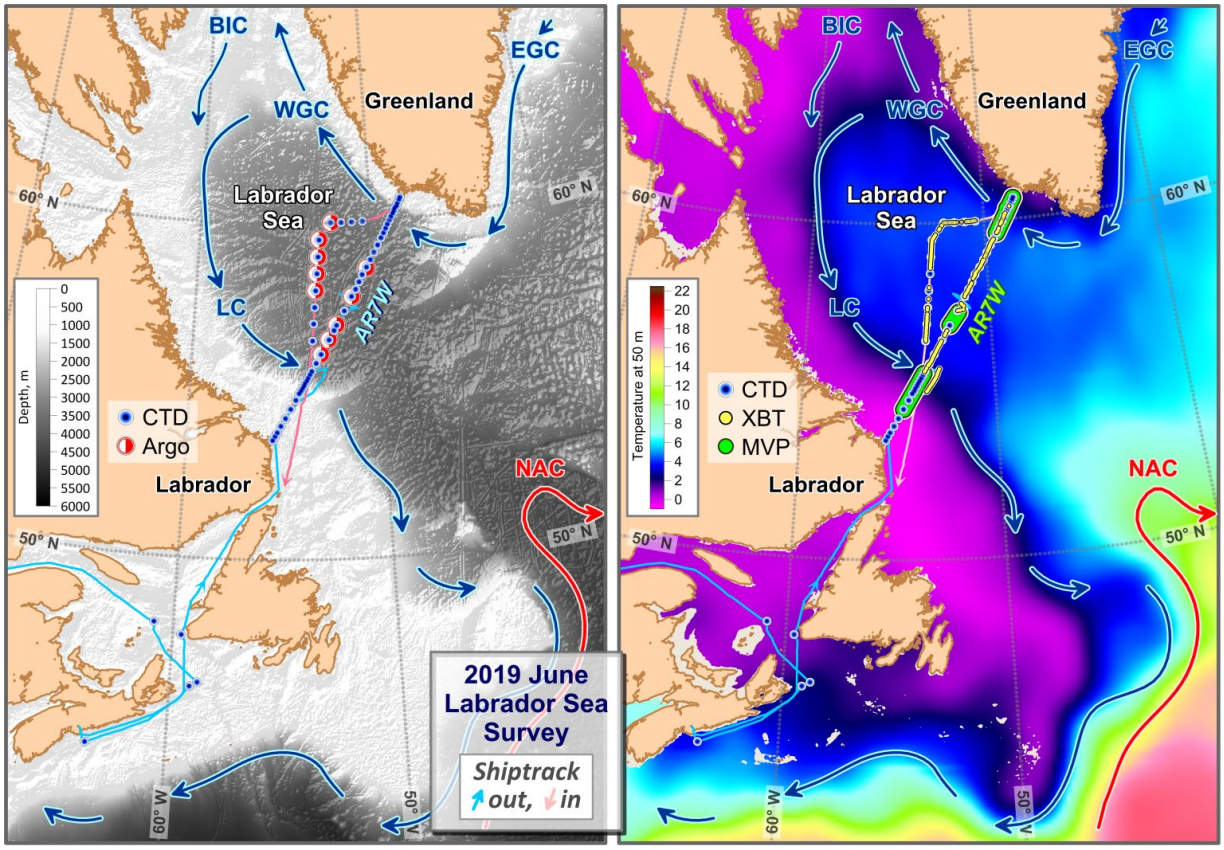

Figure 1. Topography (left panel), long-term mean temperature at 50 m (right panel) and major deep-water currents in the Labrador Sea and adjacent regions of the North Atlantic. The 2019 June Labrador Sea mission CTD stations (both panels), Argo float deployment sites (left panel), Expendable Bathythermograph (XBT) profiles (right panel) and Moving Vessel Profile (MVP) transects (right panel).

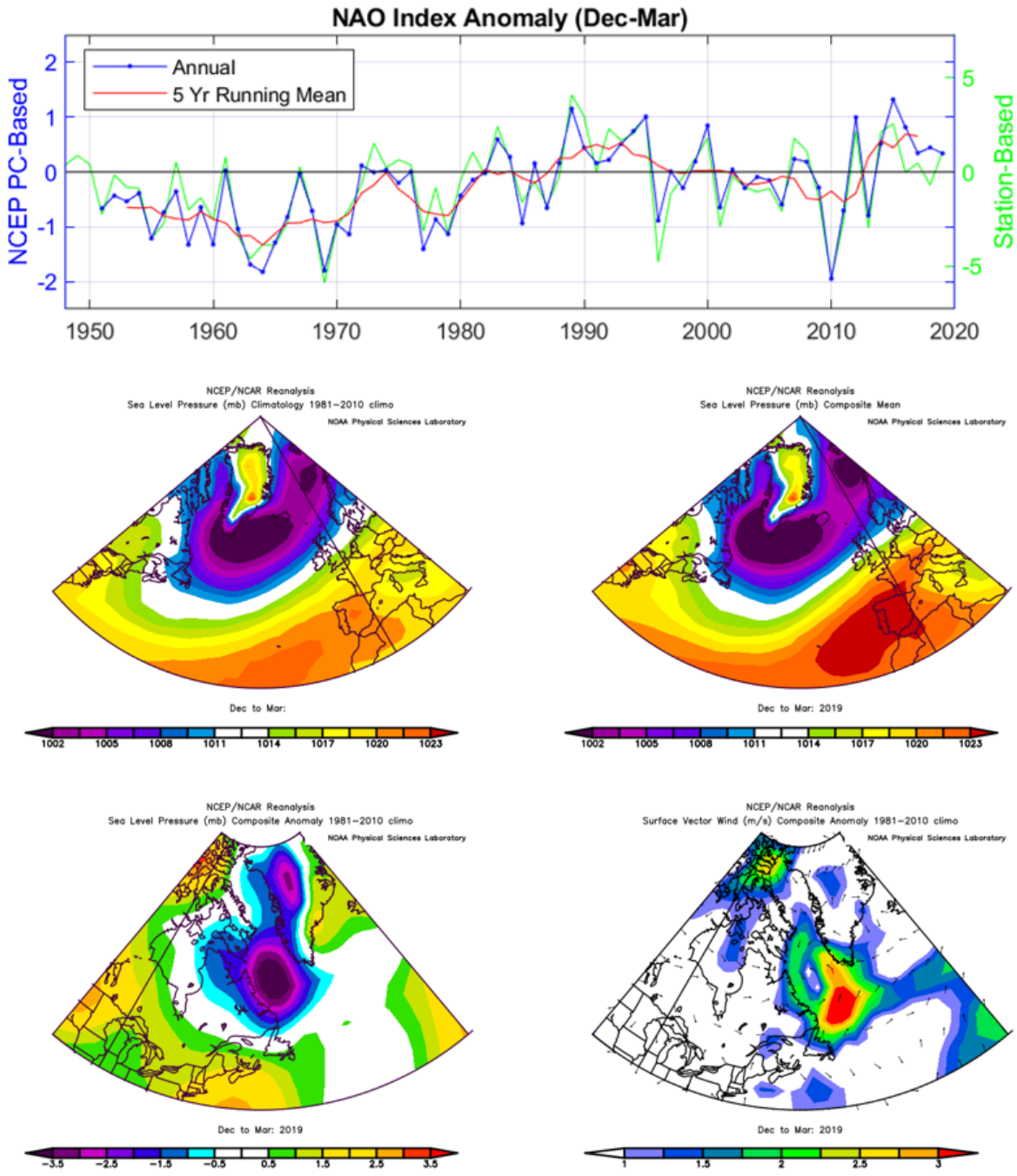

Figure 2. Anomalies of the North Atlantic Oscillation (NAO) index, relative to the 1981–2010 mean. The station-based NAO index (green) is defined as the winter (December, January, February, March) sea level pressure difference between the Azores and Iceland; data were obtained from Climate Data Guide. The principal component (PC)-based NAO index (blue) is associated with the first Empirical Orthogonal Function (EOF) of standardized monthly 500-mb height anomaly fields for the Northern Hemisphere; data were obtained from Climate Prediction Centre. The middle panels show the 1981–2010 December–March mean (middle left panel) and 2019 December–March sea-level pressure (middle right panel) over the North Atlantic. The lower panels show the 2019 December–March SLP anomaly (lower left panel) and the 2019 December–March surface-vector wind anomaly (lower right panel).

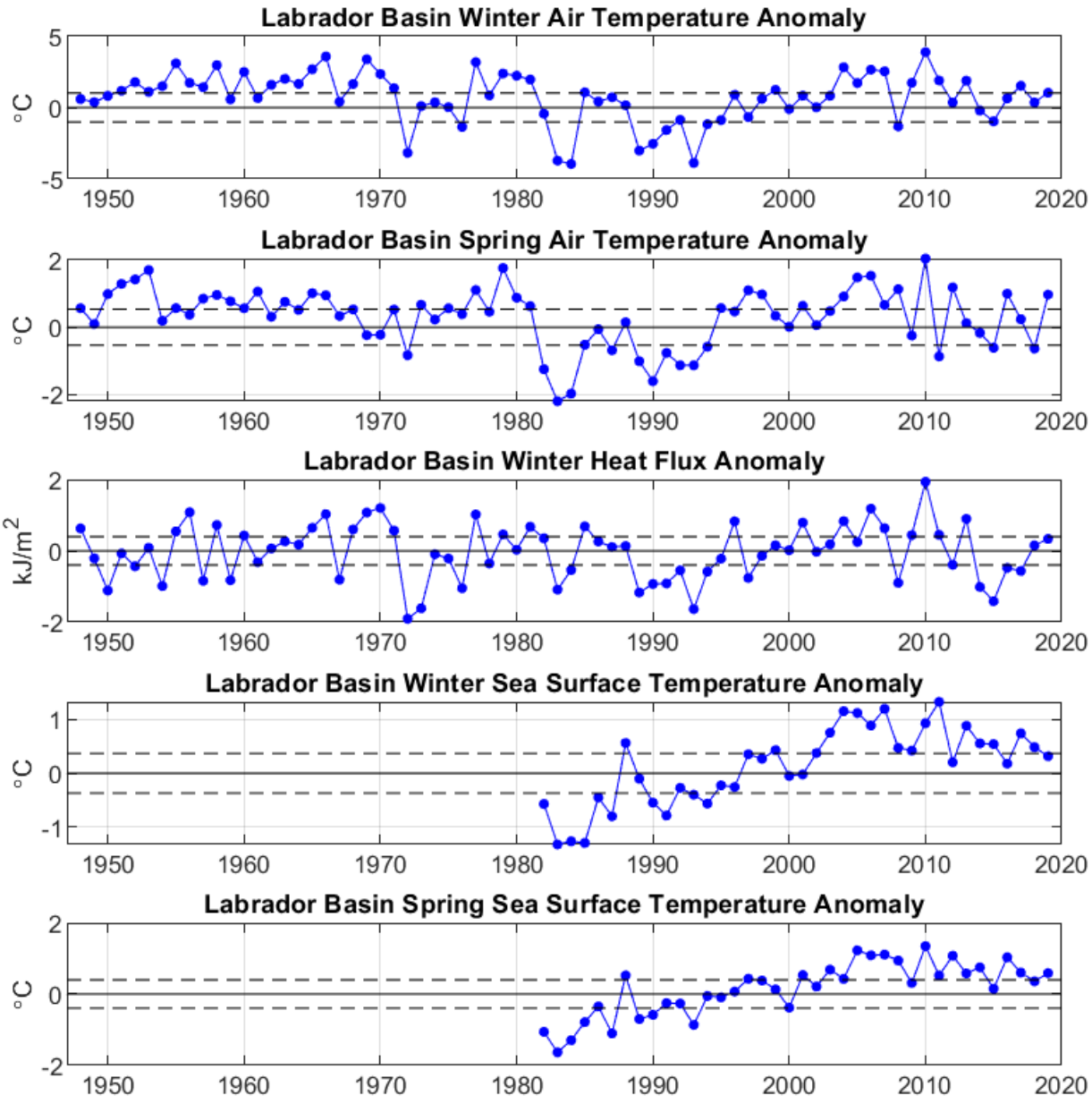

Figure 3. Anomalies of Labrador Basin winter and spring air temperature, cumulative winter surface heat flux, and winter and spring sea surface temperature, relative to the 1981–2010 mean. Horizontal dashed lines represent plus or minus 0.5 SD for the 1981–2010 period.

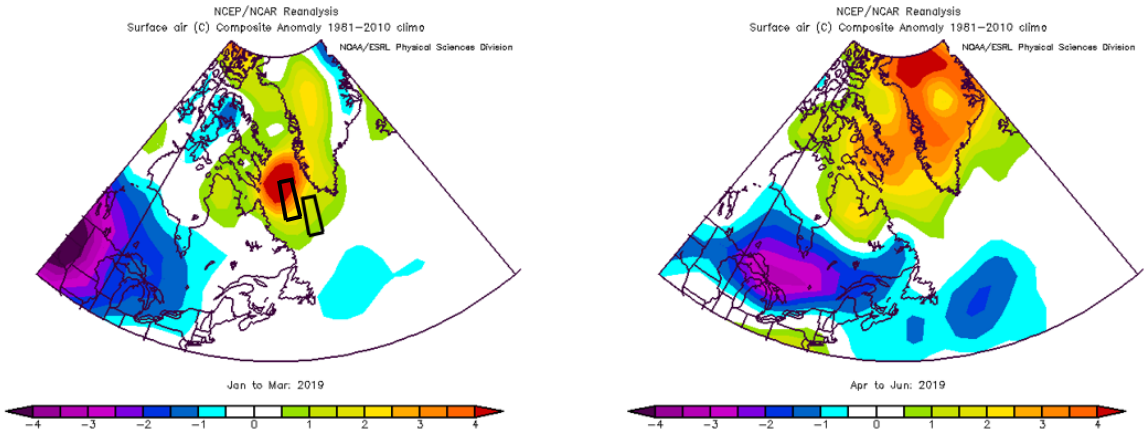

Figure 4. Winter and spring air temperature anomalies (ºC) over the Northwest Atlantic relative to the 1981–2010 means; data were obtained from NOAA Internet site (accessed 04 Feb 2020).

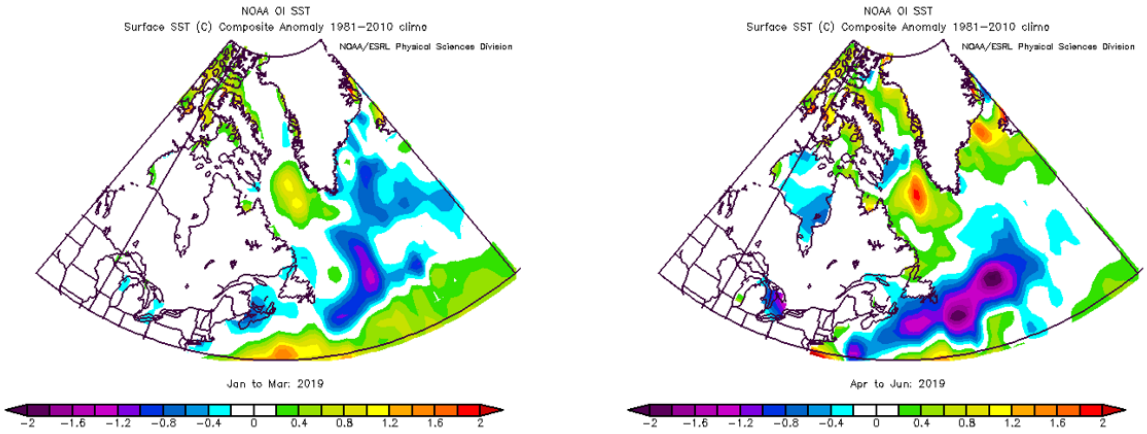

Figure 5. Winter and spring sea surface temperature anomalies (ºC) over the Northwest Atlantic relative to the 1981–2010 means; data were obtained from NOAA Internet site (accessed 04 Feb 2020).

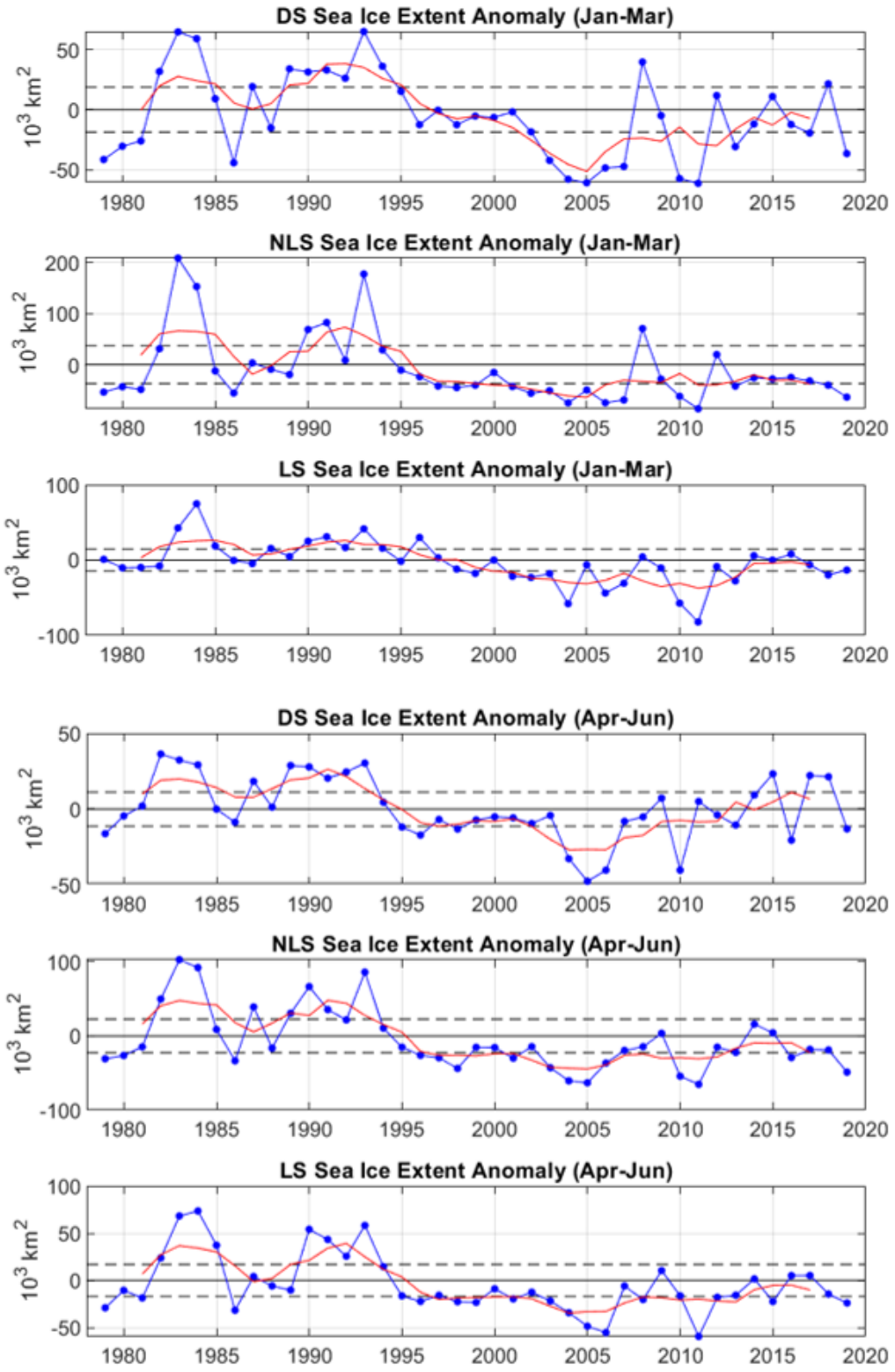

Figure 6. Winter and spring sea ice extent anomalies (blue) and their five year running means (red) for: (1) Davis Strait (DS) (63–68°N), (2) the Northern Labrador Sea (NLS) (58–63°N), and (3) Labrador Shelf (LS) (53–58°N). Horizontal dashed lines represent plus or minus 0.5 SD for the 1981–2010 period.

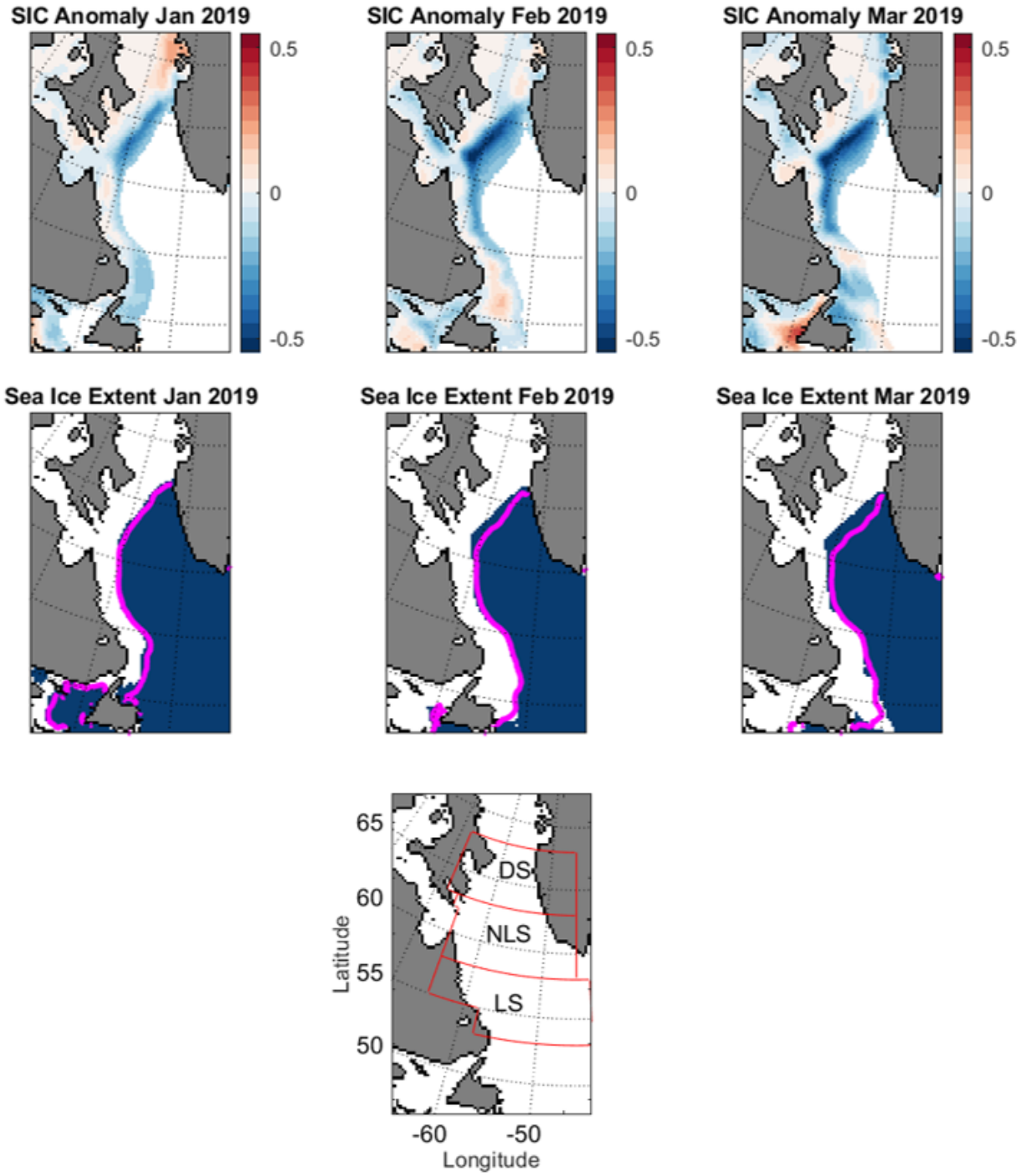

Figure 7. Sea ice concentration anomalies (top) and sea ice extent (middle) for January–March 2019 as derived by the US National Snow and Ice Data Center (reference period 1979–2000). The magenta lines show the median ice edge for 1981–2010. Davis Strait (DS), Northern Labrador Sea (NLS), and Labrador Shelf (LS) regions (bottom panel).

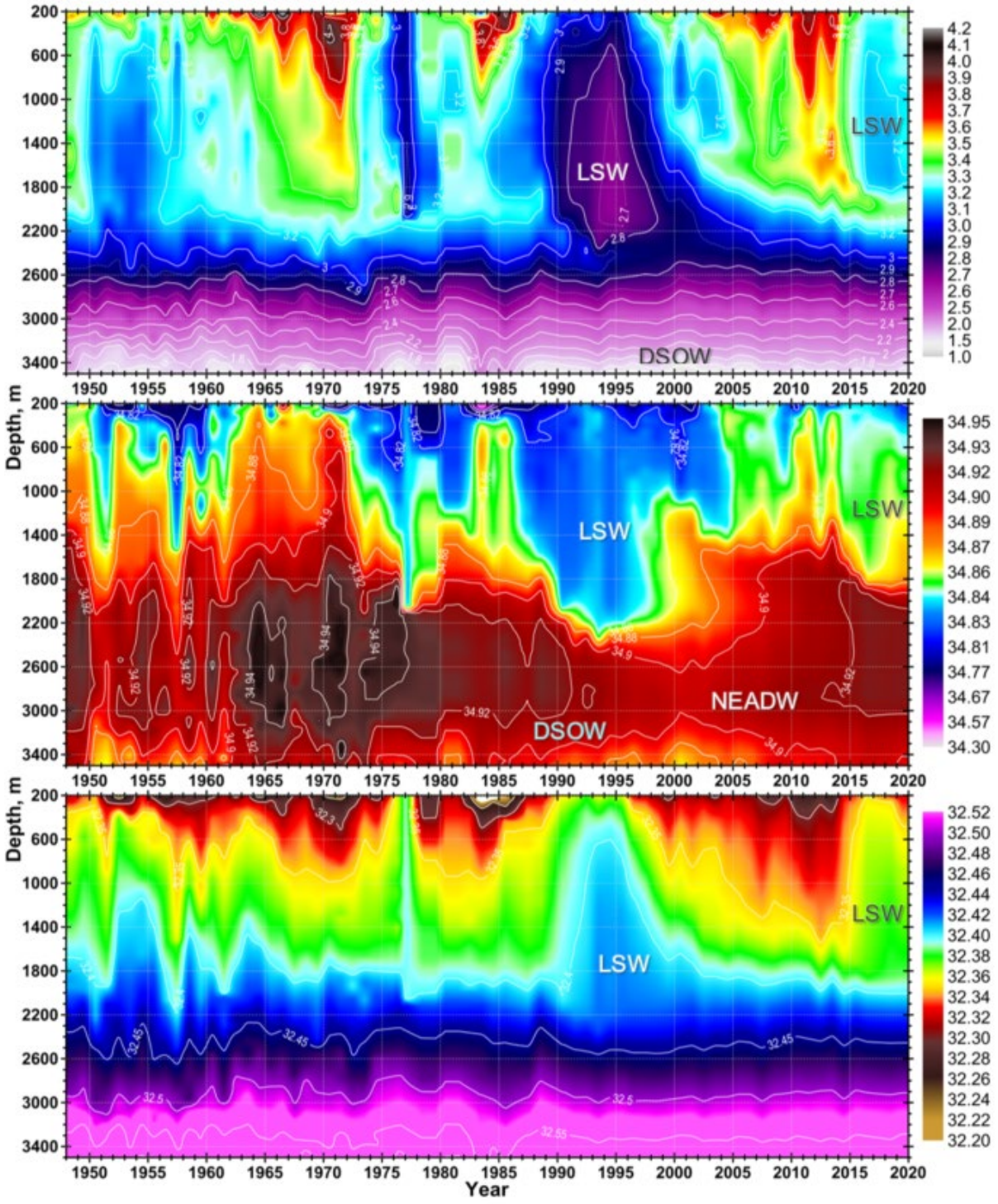

Figure 8. Annual temperature (upper panel), salinity (middle panel) and density (w.r.t. 1,000 dbar, lower panel) means in the central region of the Labrador Sea between 200 and 3,500 m based on profiling Argo float and shipboard observations for the time period of 1948–2019. LSW, NEADW, and DSOW indicate Labrador Sea Water, Northeast Atlantic Deep Water, and Denmark Strait Overflow Water, respectively.

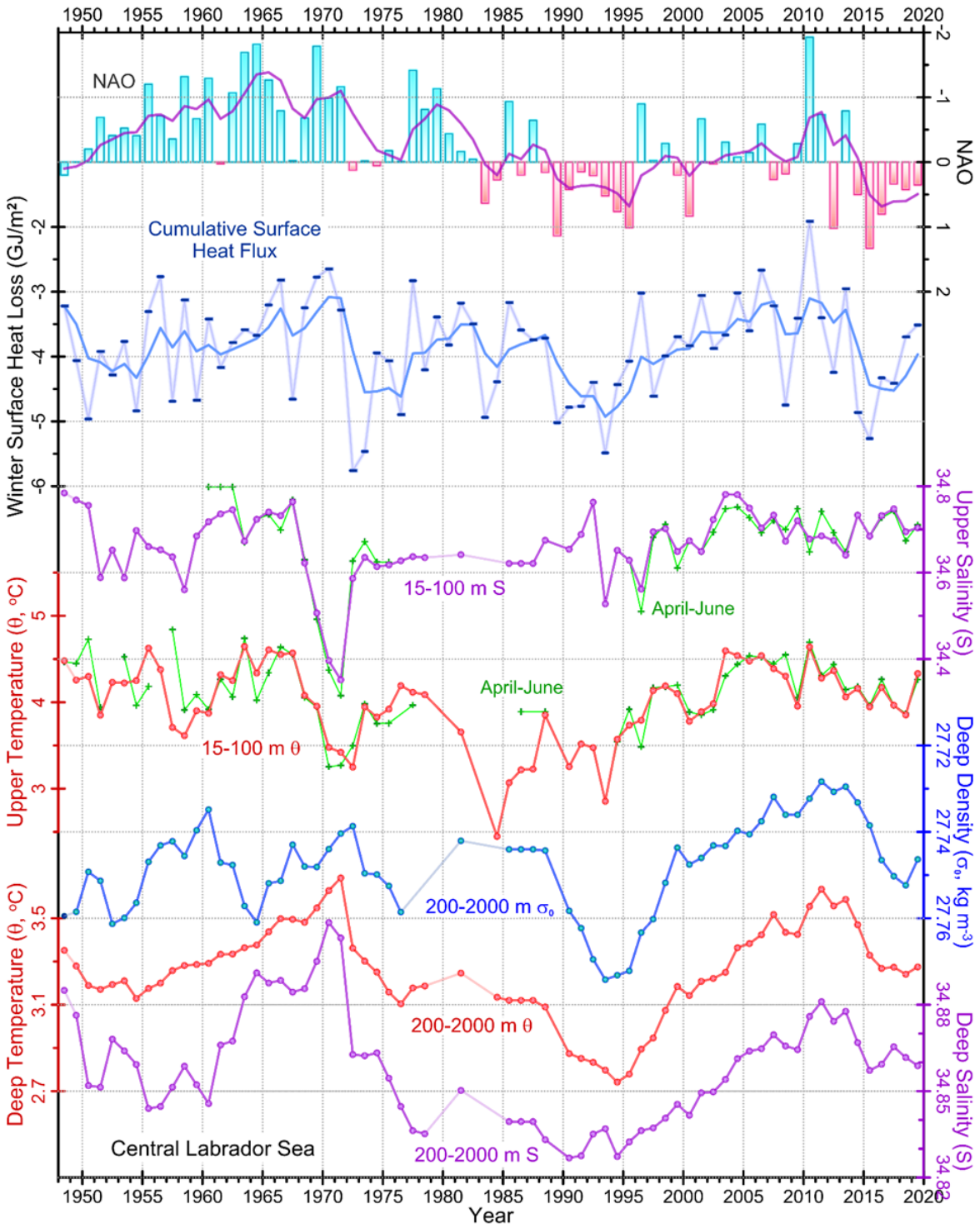

Figure 9. Major environmental indices for the central Labrador Sea since 1948. From top down: the normalized winter (North Atlantic Oscillation) NAO index (upper bar graph, inverted scale); the National Centers for Environmental Prediction (NCEP)-based cumulative surface-heat flux computed for the central Labrador Sea over individually-defined annual cooling seasons (blue); the upper two solid lines indicate five-back-point filtered series; annual and spring mean temperature (θ) and salinity (S) averaged over the 15–100 m depth range; and annual mean θ, S, and density (σ_0, w.r.t. 0 dbar) averaged over the 200–2,000 m depth range in the central Labrador Sea.

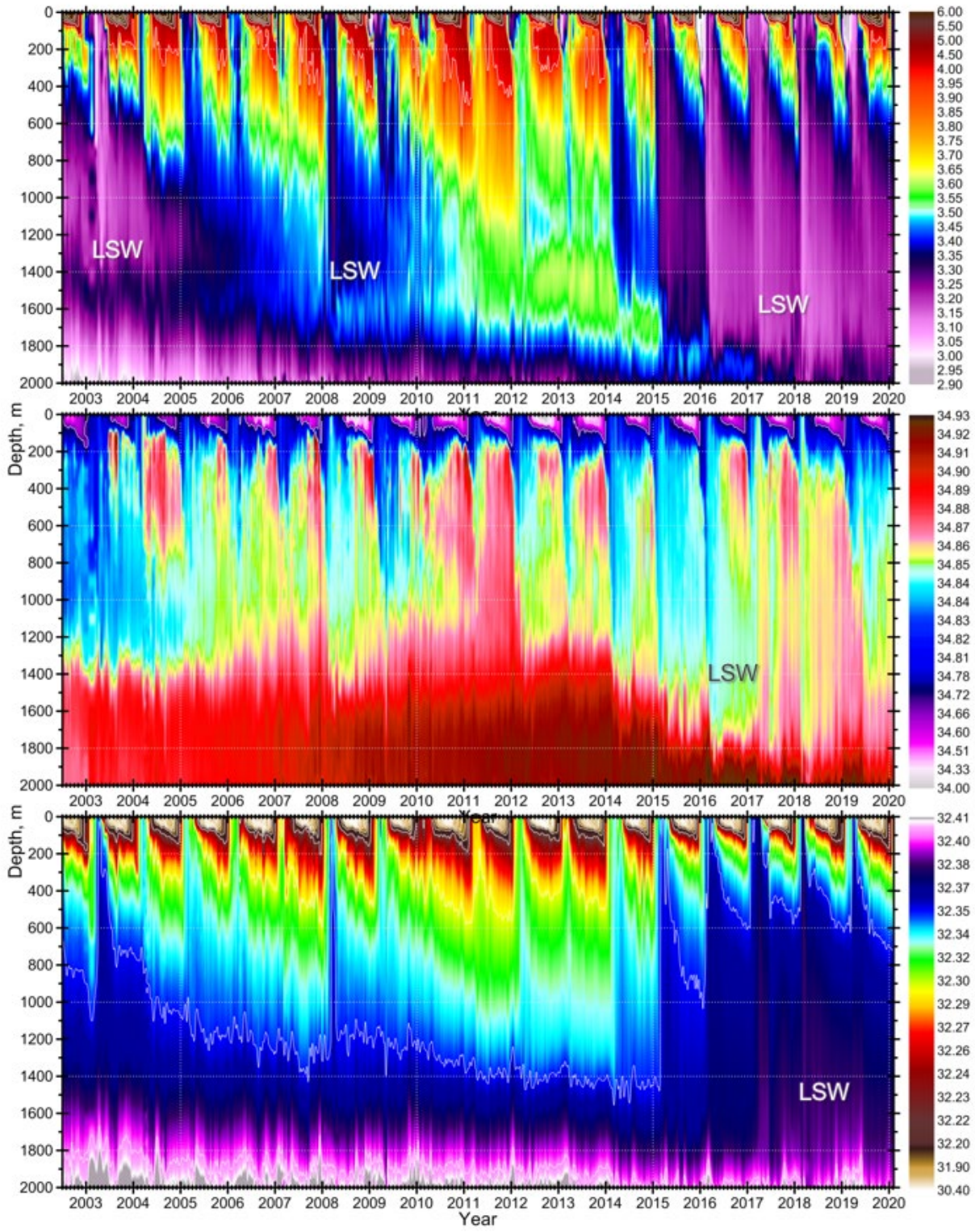

Figure 10. Variability of temperature (upper panel), salinity (lower panel), and density (middle panel) in the central region of the Labrador Sea based on profiling Argo float and research vessel survey data from 0 to 2,000 m for the time period of 2002–2020 averaged in 10-day time bins spaced at 5-day intervals.

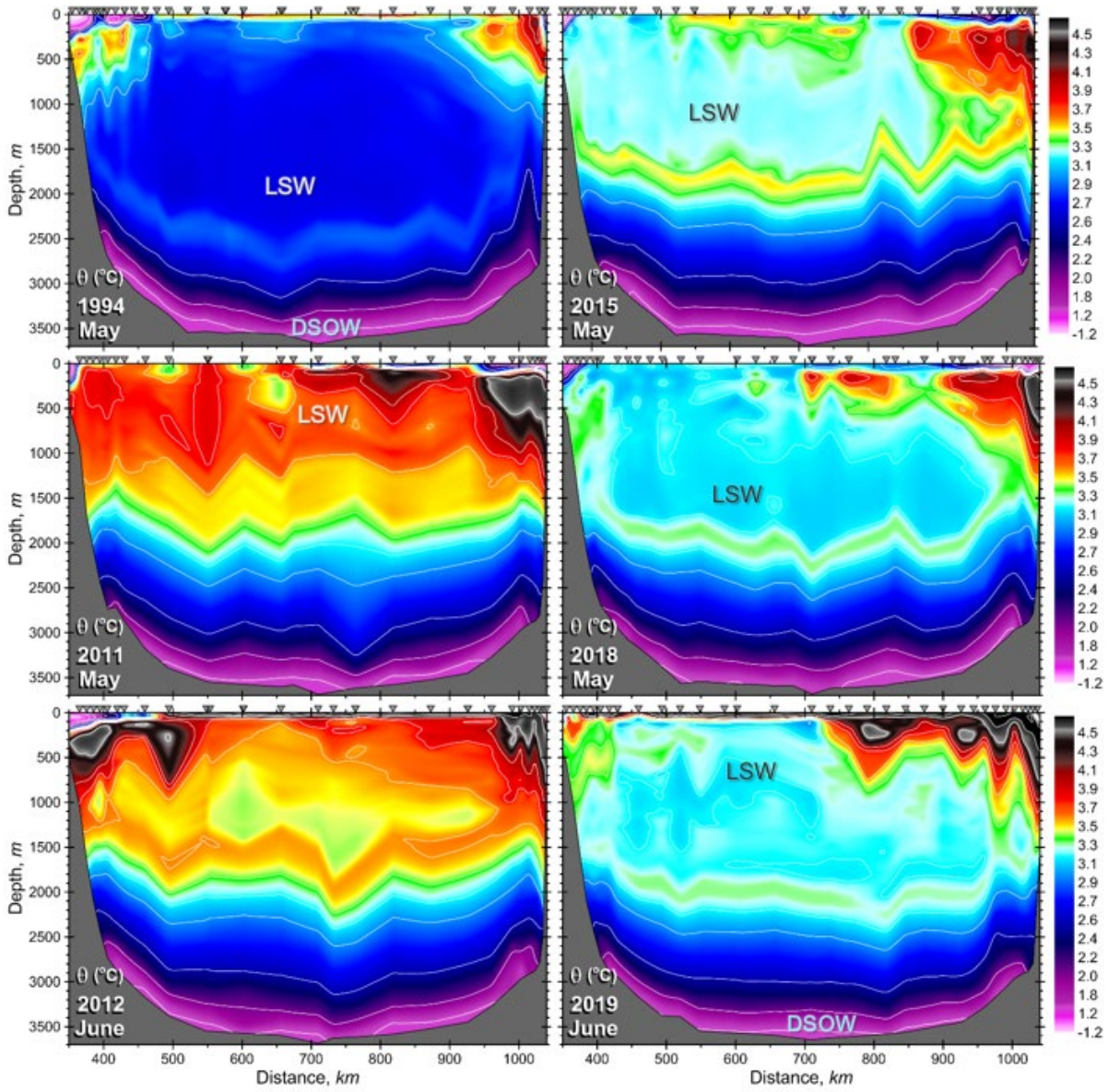

Figure 11. Distributions of potential temperature (θ, °C) on the Atlantic Repeat 7-West (AR7W) line across the Labrador Sea from annual spring-summer surveys in 1994, 2011, 2012, 2015, 2018, and 2019. Inverted triangles along the top of each panel indicate station locations. LSW, NEADW, and DSOW indicate Labrador Sea Water, Northeast Atlantic Deep Water and Denmark Strait Overflow Water, respectively.

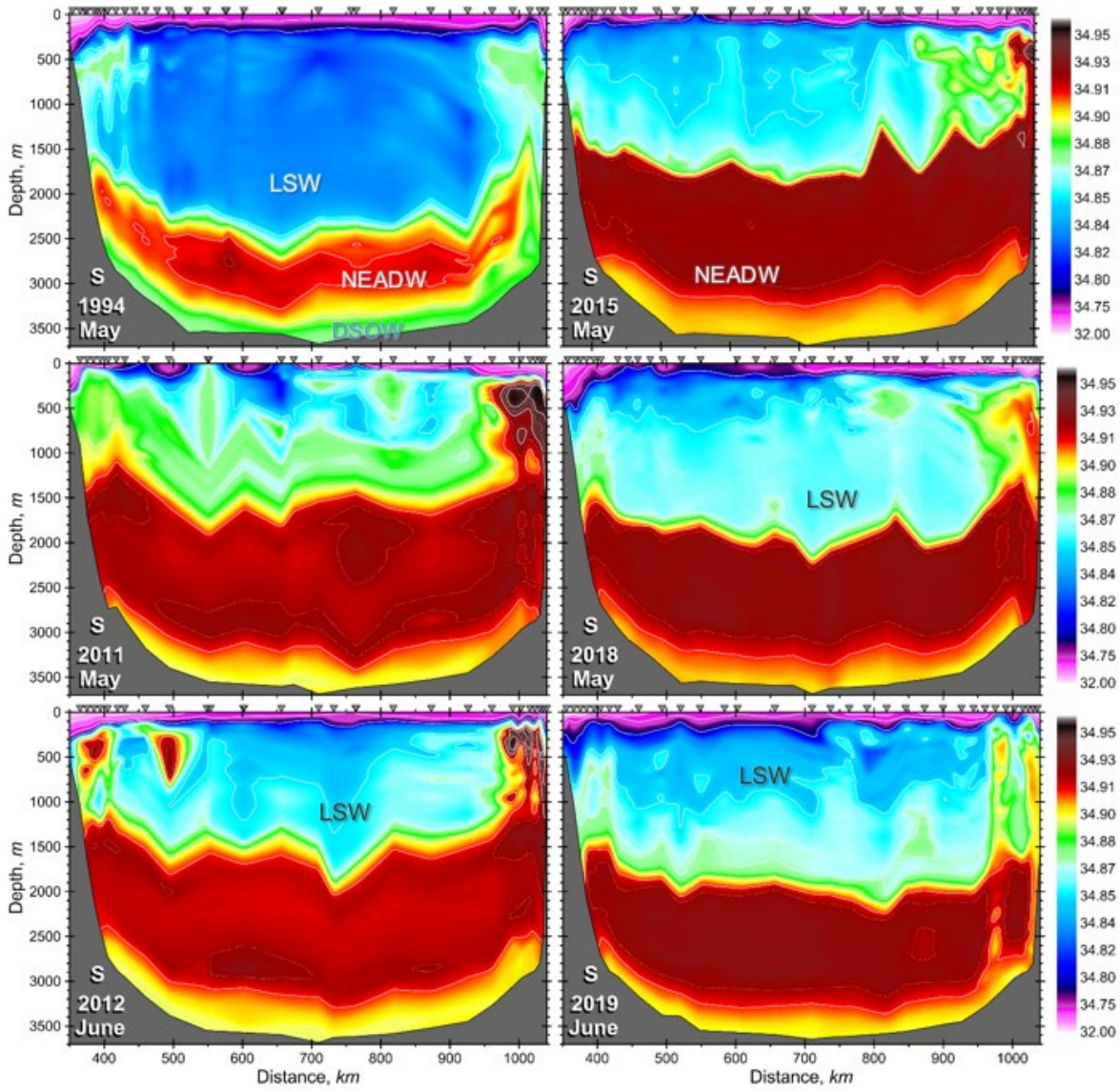

Figure 12. Distributions of salinity (S) on the Atlantic Repeat 7-West (AR7W) line across the Labrador Sea from annual spring-summer surveys in 1994, 2011, 2012, 2015, 2018, and 2019. Inverted triangles along the top of each panel indicate station locations. LSW, NEADW, and DSOW indicate Labrador Sea Water, Northeast Atlantic Deep Water, and Denmark Strait Overflow Water, respectively.

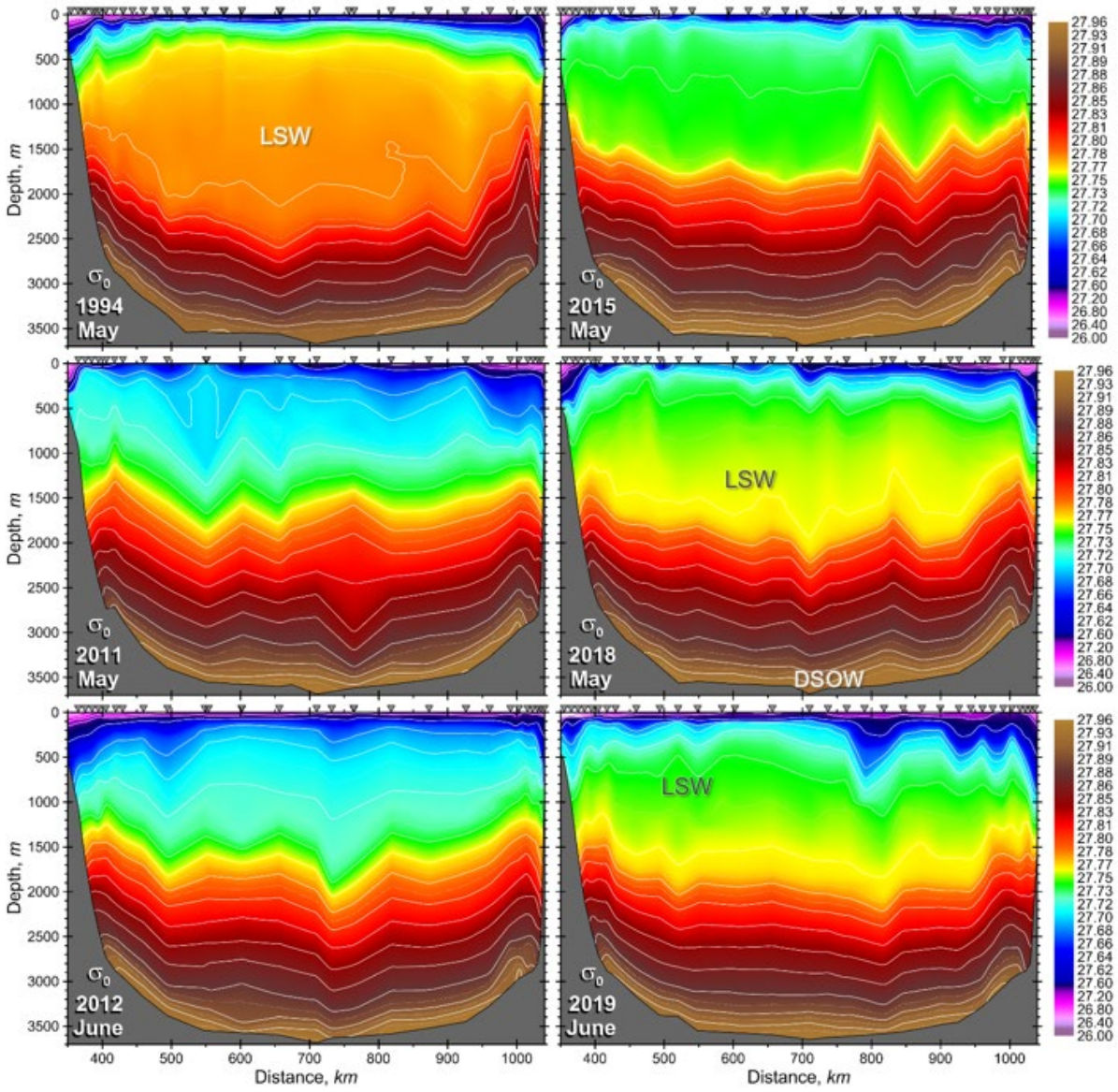

Figure 13. Distributions of potential density (σ_o, referenced to the sea surface, kg/m^3) on the Atlantic Repeat 7-West (AR7W) line across the Labrador Sea from annual spring-summer surveys in 1994, 2011, 2012, 2015, 2018, and 2019. Inverted triangles along the top of each panel indicate station locations. LSW, NEADW, and DSOW indicate Labrador Sea Water, Northeast Atlantic Deep Water, and Denmark Strait Overflow Water, respectively.

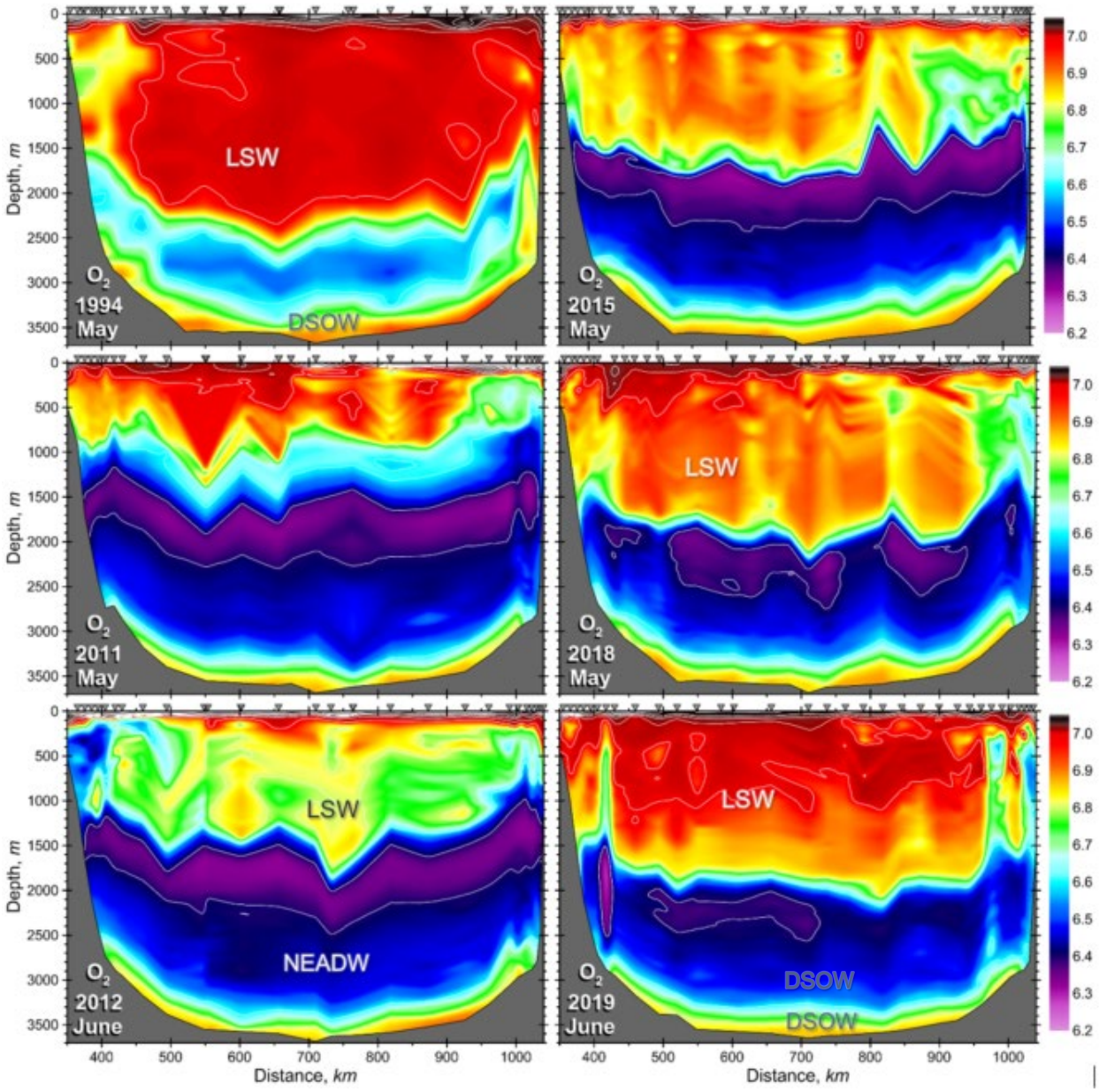

Figure 14. Distributions of dissolved oxygen (ml/l) on the Atlantic Repeat 7-West (AR7W) line across the Labrador Sea from annual spring-summer surveys in 1994, 2011, 2012, 2015, 2018, and 2019. Inverted triangles along the top of each panel indicate station locations. LSW, NEADW, and DSOW indicate Labrador Sea Water, Northeast Atlantic Deep Water, and Denmark Strait Overflow Water, respectively.

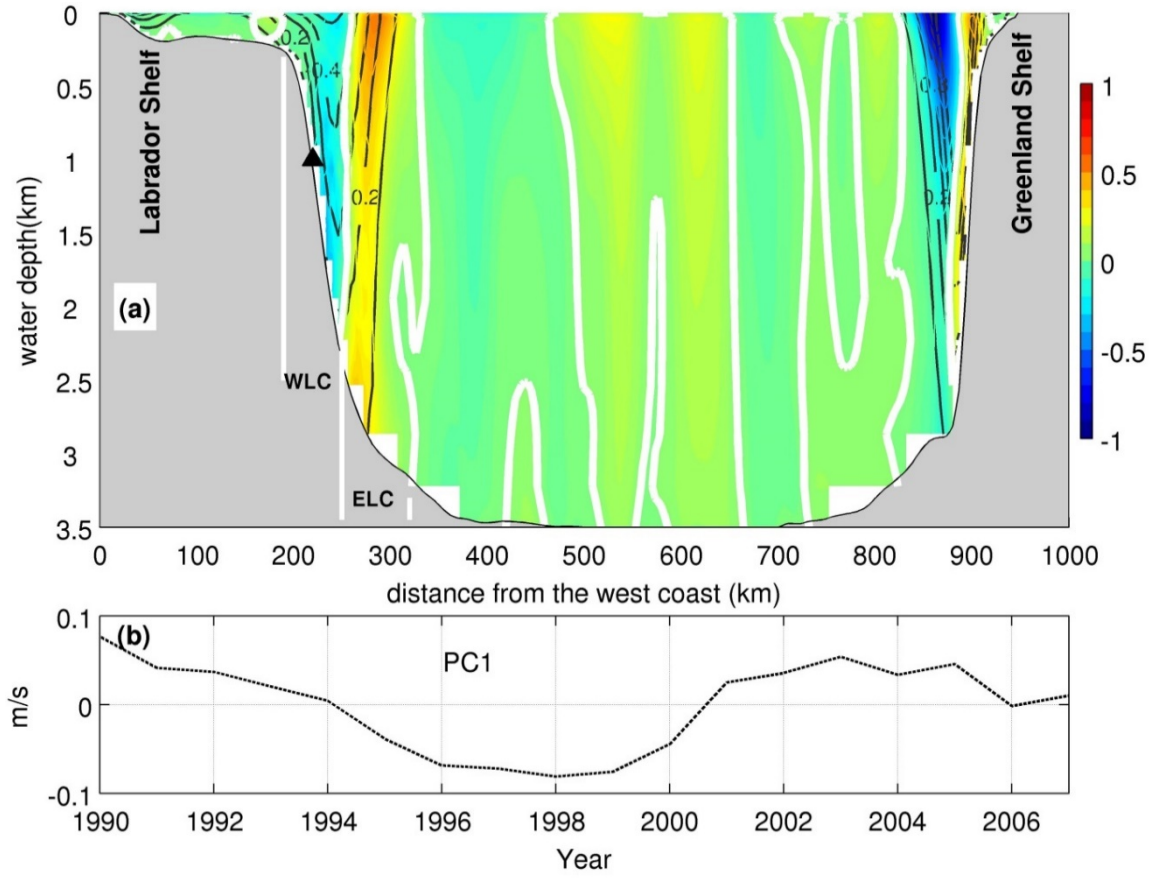

Figure 15. (a) Empirical Orthogonal Function 1 (EOF1) pattern of the normal velocities along Atlantic Repeat 7-West (AR7W) (based on results from 1990 to 2007). The shaded areas represent the EOF pattern, bold white lines are zeros contours of the EOF pattern, the black labeled lines are the mean normal velocities (in m/s). Note: positive direction is northward. The black triangle indicates the location of the mooring referred to in the text. (b) Corresponding principal component 1 (PC1).

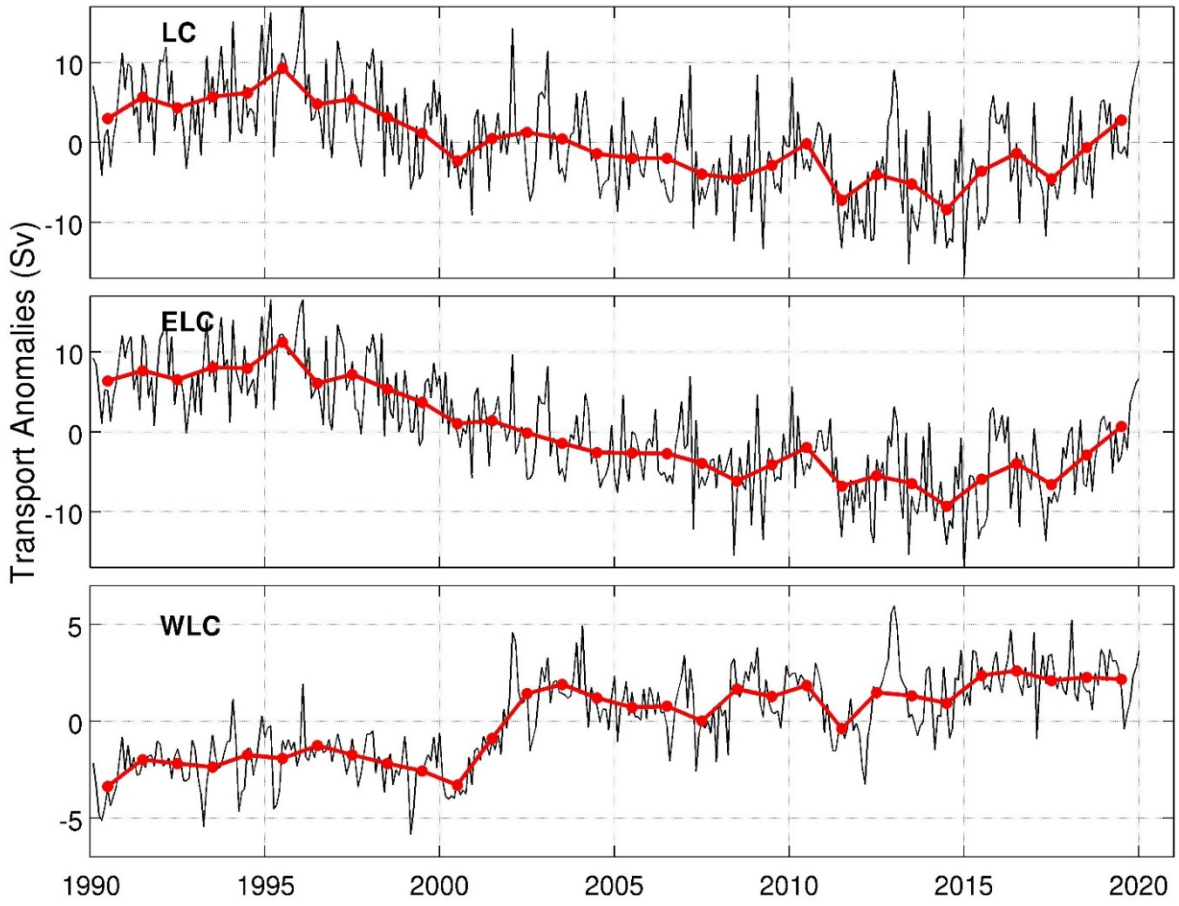

Figure 16. Transport anomalies of the Labrador Current (LC), Eastern Labrador Current (ELC), and Western Labrador Current (WLC) from 1990 to 2019.
Note: black lines are from the monthly data, and red lines and dots are from the annual means.

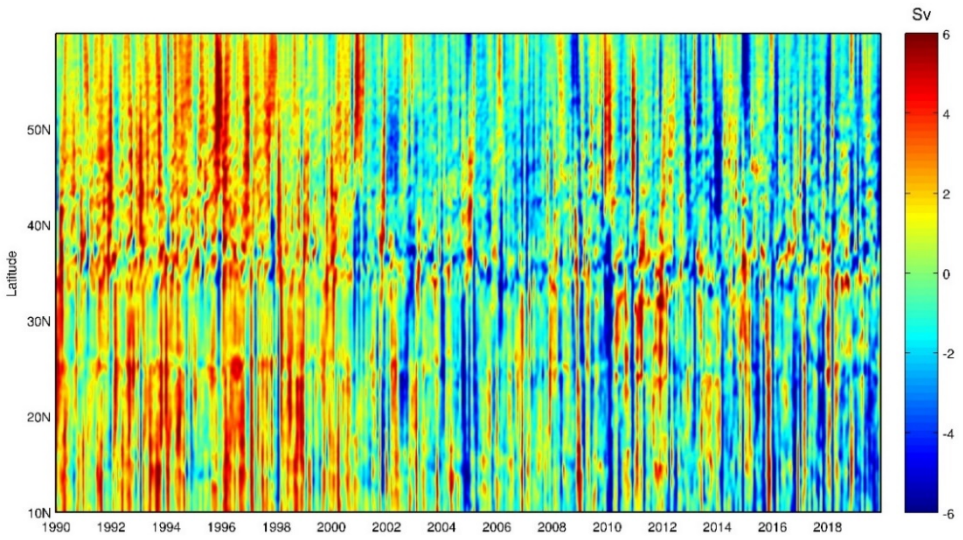

Figure 17. The Atlantic Meridional Overturning Circulation (AMOC) anomalies at different latitudes with the seasonal cycles removed, but without detrending.

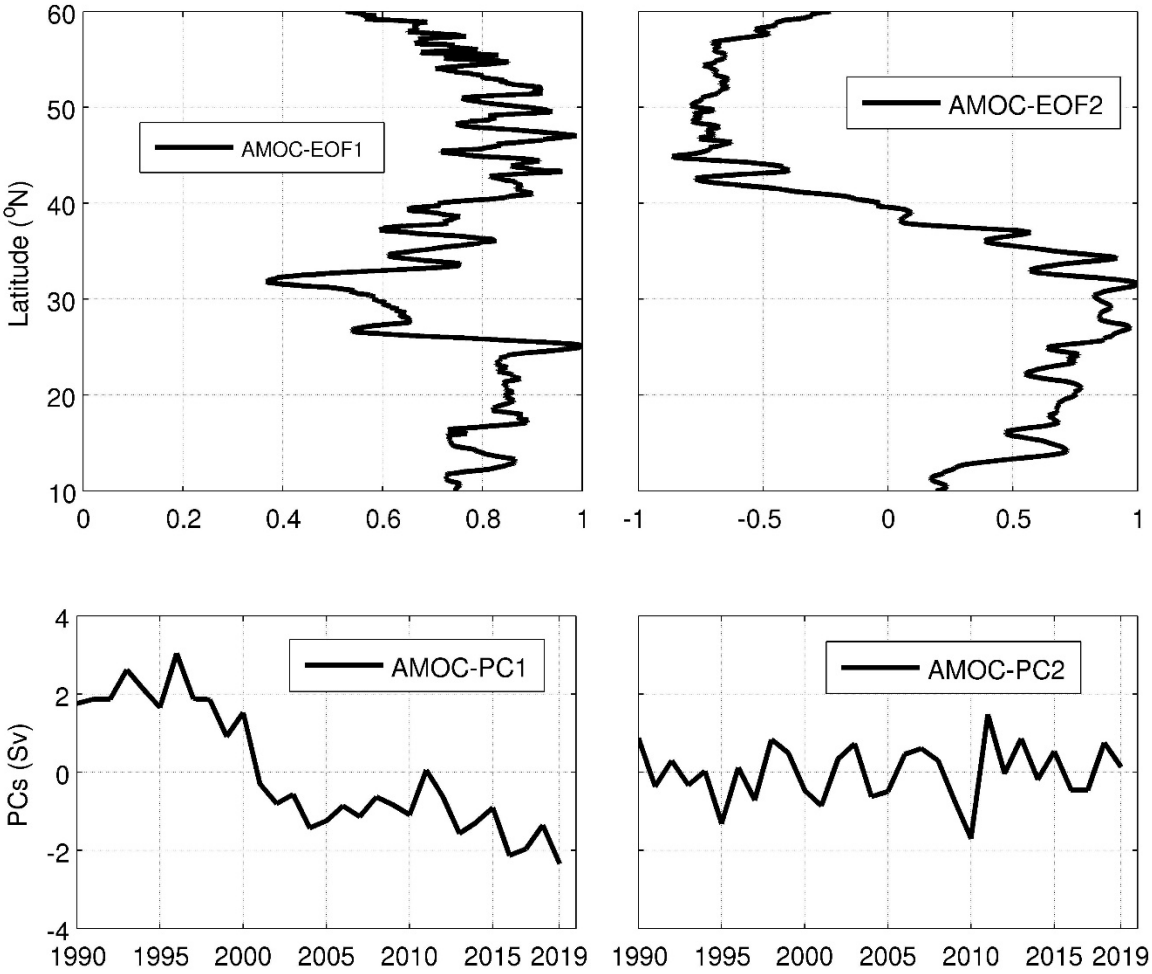

Figure 18. Empirical Orthogonal Function (EOF) patterns of Atlantic Meridional Overturning Circulation (AMOC) (top panel) and associated principal components (PCs) of these EOFs (bottom panel).

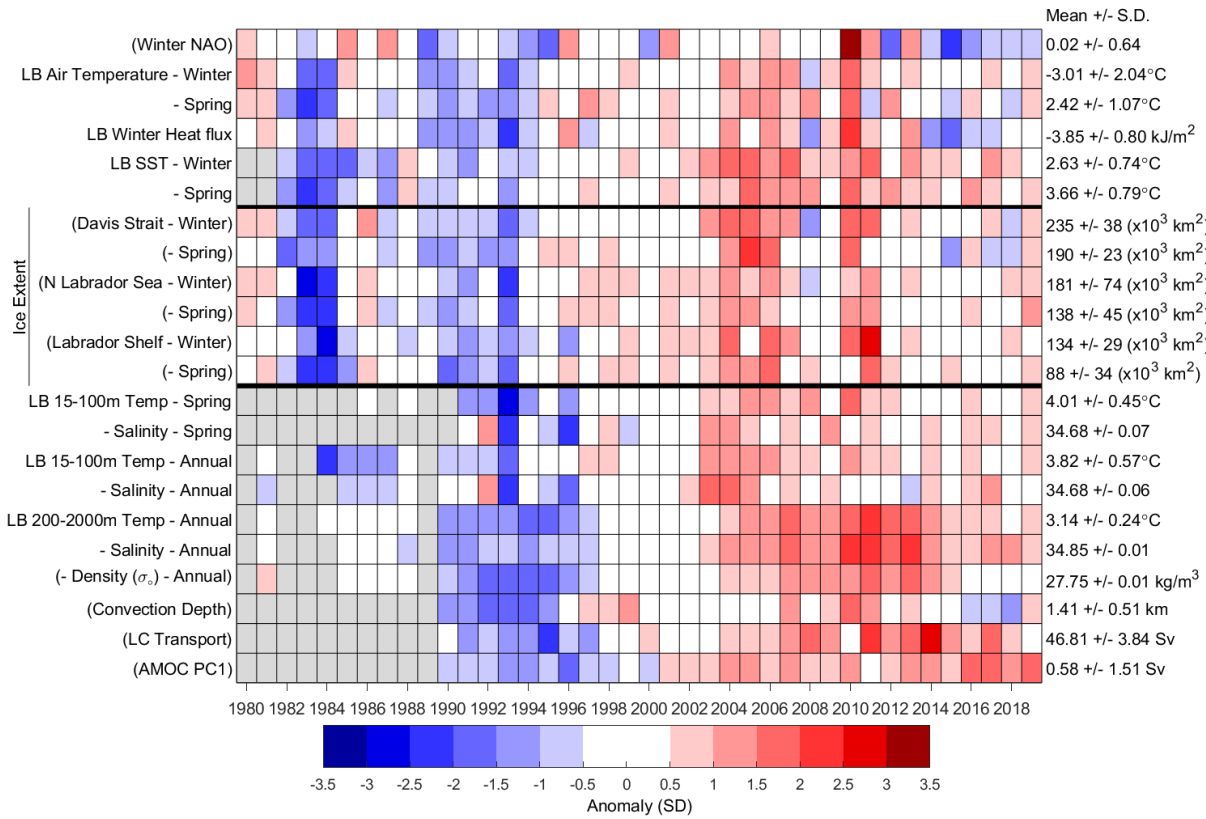

Figure 19. Scorecard for 1980–2019 oceanographic series. A grey cell indicates missing data, a white cell is a value within 0.5 Standard Deviation (SD) of the long-term mean based on data from 1981–2010 when possible; a red cell indicates above normal conditions, and a blue cell below normal. Variables whose names appear in parentheses have reversed colour coding, whereby reds are lower than normal values that correspond to warm conditions. More intense colours indicate larger anomalies. Long-term means and standard deviations are shown on the right-hand side of the figure. North Atlantic Oscillation [NAO], Labrador Basin [LB], Labrador Current [LC].

APPENDIX

SEASONAL CYCLE AS A SOURCE OF ERROR IN OCEAN STATE ASSESSMENTS

Figures A1-5 show the regular seasonal cycles of temperature and salinity (A1), the associated seasonal changes encountered in 30 days (A2) and seasonal changes measured from May 15 (A3), standard deviations of anomalies in 10-day bins (A4) and contributions of the seasonal cycles to the total variances (A5). The estimates included in these figures are based on iterative evaluation of seasonal cycle using irregular data analysis routines (Yashayaev, 2001). The seasonal warming that occurs over a 30-day May period, coinciding with May, is much larger than the standard deviation of temperature anomalies, meaning that the seasonally-imposed scatter would be large, if a time series was constructed for the upper 100 m layer without applying a seasonal correction. Furthermore, the trend in survey date noted above (Table 1) would lead to a systematic seasonal bias in a long time series forming an artificial trend, if the seasonal was not properly removed from the observations.

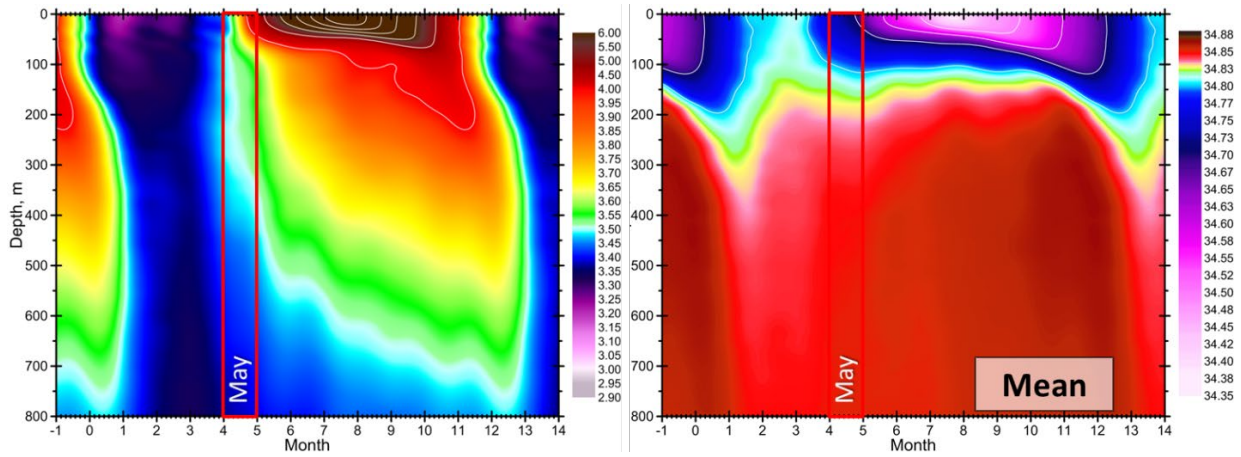

Figure A1. Regular seasonal cycles of temperature (left) and salinity (right) in the central Labrador Sea based on the iterative time series analysis technique by Yashayaev.

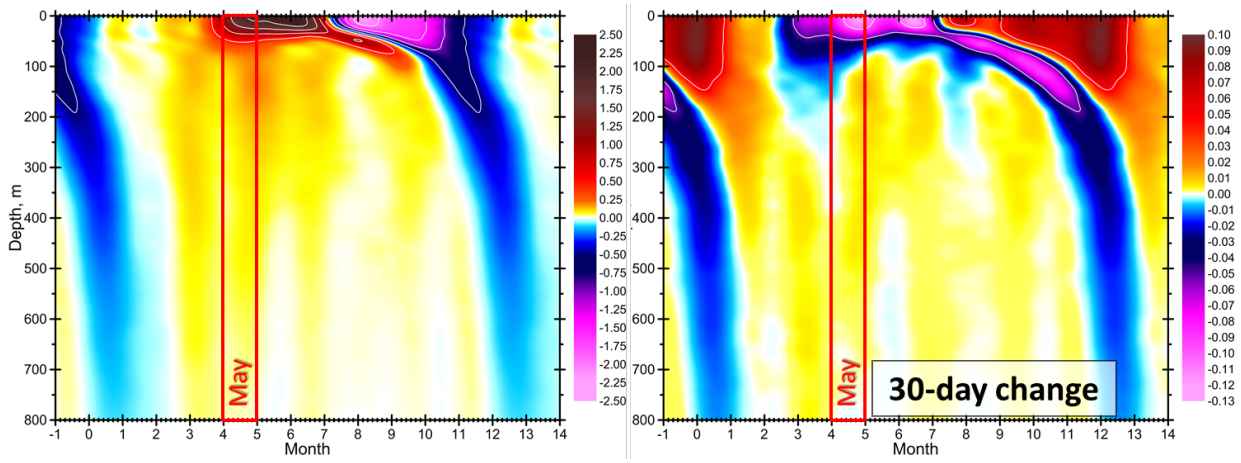

Figure A2. Seasonal changes of temperature (left) and salinity (right) encountered over 30-day periods.

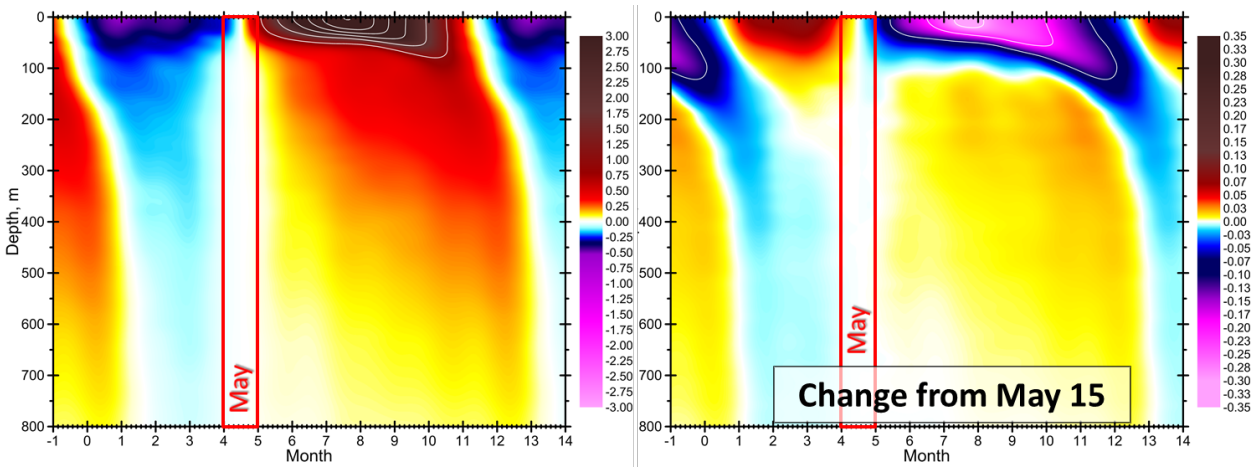

Figure A3. Seasonal changes of temperature (left) and salinity (right) measured from May 15.

.

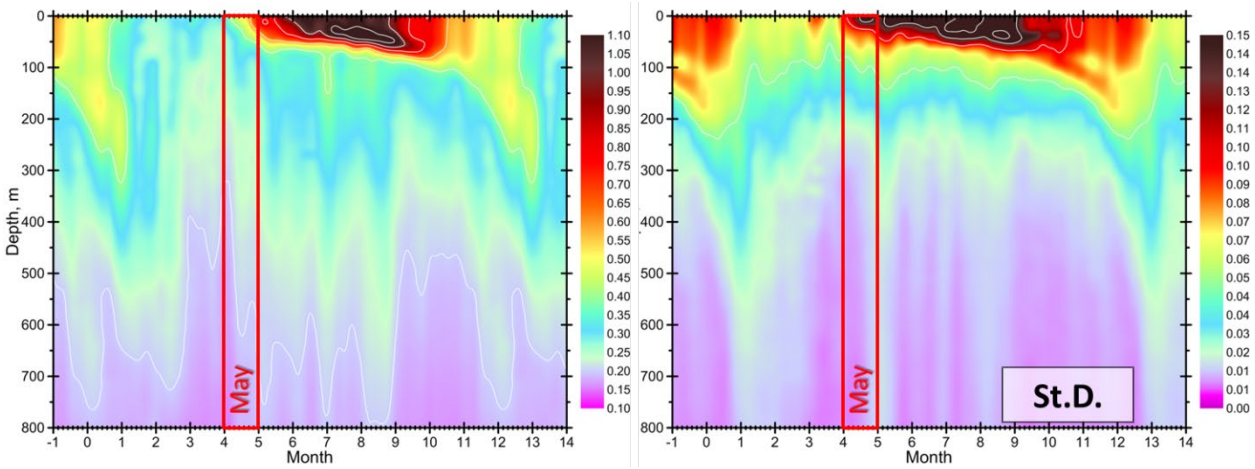

Figure A4. Standard deviations of temperature (left) and salinity (right) anomalies in the central Labrador Sea computed in 10-day time bins spaced at 5-day intervals. The anomalies were computed by subtracting the harmonic seasonal cycle (Figure A1) from all multiyear observations at each depth. The data have been quality controlled (outliers removed) using the iterative seasonal cycle estimation techniques. Note that the standard deviations of temperature anomalies is smaller than the 30-day seasonal temperature change in May (Figure A2).

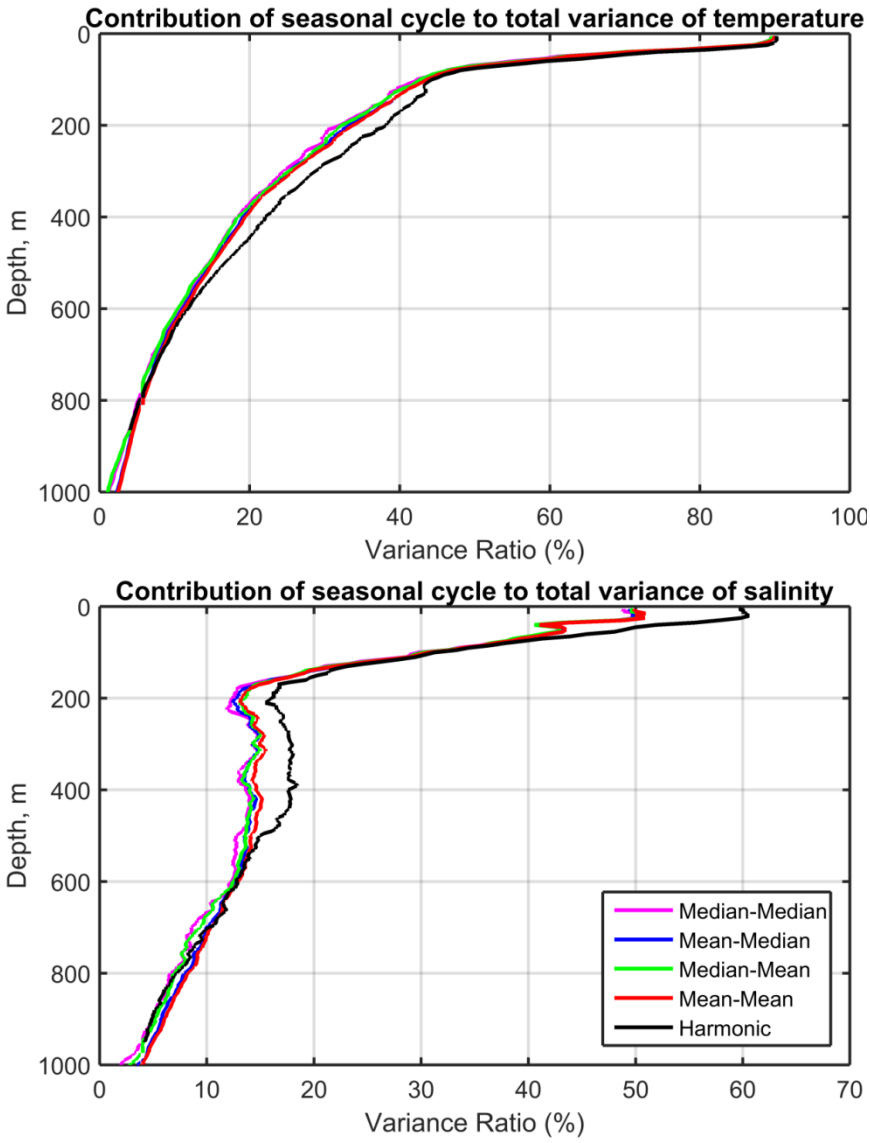

Figure A5. Contribution of computed seasonal cycle to the total variance of temperature (top) and salinity (bottom). The seasonal cycles were estimated by using data binning with 10-day bins spaced at 5-day intervals (coloured lines) and by using the iterative time series analysis technique based on harmonic analysis (black line) developed by Yashayaev. The data have been quality-controlled (outliers removed) as part of the same time series analysis. The contributions are computed by dividing the variance of the respective seasonal cycle by the total variance and multiplying by 100%. This measure, for example, indicates that 90% of the total temperature variance at the sea surface is associated with the seasonal cycle. The contribution of the seasonal cycle below 200 m is less than 40% for temperature and less than 20% for salinity, and it rapidly declines with depth. This means that the annual averaging is permissible without applying a seasonal correction only below 200–300 m, but not above.